Title

tBeam—A Fast Model to Estimate Energy Consumption Due to Pavement Structural Response: Theoretical and Validation Manual

Authors

Weissman, Shmuel L.
Kelly, James M.

Publication Date

2021-06-01

DOI

10.7922/G2P26WF2

June 2021
Reprint Report: UCPRC-RP-2021-02

tBeam—
A Fast Model to Estimate Energy Consumption Due to Pavement Structural Response

Theoretical and Validation Manual

Author:
Shmuel L. Weissman and James M. Kelly, Symplectic Engineering Corporation

This report is based on research performed by the Symplectic Engineering Corporation on behalf of the University of California Pavement Research Center for the California Department of Transportation, and is reprinted here in its original form.

Work Conducted as part of University of California Research Agreement #201702289-03

PREPARED FOR:

California Department of Transportation
Division of Research, Innovation, and System Information
Office of Materials and Infrastructure

PREPARED BY:

University of California
Pavement Research Center
UC Davis, UC Berkeley

TECHNICAL REPORT DOCUMENTATION PAGE

1. REPORT NUMBER UCPRC-RP-2021-02	2. GOVERNMENT ASSOCIATION NUMBER	3. RECIPIENT'S CATALOG NUMBER
4. TITLE AND SUBTITLE tBeam—A Fast Model to Estimate Energy Consumption Due to Pavement Structural Response: Theoretical and Validation Manual		5. REPORT PUBLICATION DATE June 2021 6. PERFORMING ORGANIZATION CODE
7. AUTHOR(S) Shmuel L. Weissman and James M. Kelly		8. PERFORMING ORGANIZATION REPORT NO. UCPRC-RP-2021-02 UCD-ITS-RR-21-33
9. PERFORMING ORGANIZATION NAME AND ADDRESS Symplectic Engineering 2901 Benvenue Avenue Berkeley, CA 94705		10. WORK UNIT NUMBER 11. CONTRACT OR GRANT NUMBER UC subcontract number #201702289-03 as part of Caltrans contract number 65A0628
12. SPONSORING AGENCY AND ADDRESS California Department of Transportation Division of Research, Innovation, and System Information P.O. Box 942873 Sacramento, CA 94273-0001		13. TYPE OF REPORT AND PERIOD COVERED Reprint Report November 2017 to July 2020 14. SPONSORING AGENCY CODE

15. SUPPLEMENTAL NOTES
DOI: 10.7922/G2P26WF2

16. ABSTRACT

One of the most important contributors to the environmental impacts from use of highways is the energy exerted by vehicles, particularly routes that carry higher volumes of traffic. Part of this energy is consumed by response of the the vehicle's tires and suspension to pavement surface roughness and macrotexture. Another part of the energy consumed is by energy dissipation due to the structural response of the pavement itself under the moving load. This document is the theoretical and validation manual tor tBeam, standalone software for the analysis of energy dissipation in pavements under moving vehicles. tBeam was developed as part of the improvement of modeling capabilities for environmental life cycle assessment of pavements being conducted the University of California Pavement Research Center for the California Department of Transportation. The energy consumed due to structural response are controlled by the structural properties of the pavement which are dependent on the time of day, the season, and the condition (damage) of the pavement. The energy dissipation also depends on the speed and weight of each moving wheel load. As a result, estimating the lifetime energy dissipated in a pavement structure requires multiple analyses considering the thousands of permutations of these variables for a given segment of the highway network. Therefore, models for pavement-vehicle energy dissipation must balance two opposing needs: obtaining a reasonably accurate estimate of the dissipated energy, and high numerical efficiency. For numerical efficiency, the tBeam software employs a one-dimensional finite-element based solution of a wheel traveling at a constant velocity on a viscoelastic beam-foundation system, and a further reduction of numerical effort is obtained by formulating the model relative to a moving coordinate system attached to the wheel. The one-dimensional solution is, by nature, an approximation to the three-dimensional world. This approximation can be improved by incorporating a "correction factor," which is based on comparisons with pavement simulations accounting for the double curvature observed in loaded pavements. In this report prediction disparity for a single structure is studied. The results show a clear trend where the correction factor decreases with rising temperature, and increases with higher velocity. The present study was insufficient to establish a law for the correction factor even for the single case studied. The correction factor ranged from about 1.25 at low temperature and high velocity to about 0.6 for high temperature and low velocity. The first part of this report presents the underlying theory for tBeam and implementation details. The second part presents closed form solutions for specialized pavement-foundation systems. The third component of the report presents some of the validation simulations undertaken to demonstrate the performance of tBeam, including comparisons with closed form solutions provided in this report, and recommendations for further development of tBeam.

17. KEY WORDS pavement energy dissipation, viscoelastic, life cycle assessment, pavement-vehicle interaction, structural response	18. DISTRIBUTION STATEMENT No restrictions. This document is available to the public through the National Technical Information Service, Springfield, VA 22161	
19. SECURITY CLASSIFICATION (of this report) Unclassified	20. NUMBER OF PAGES 69	21. PRICE None

UCPRC ADDITIONAL INFORMATION

1. DRAFT STAGE Final	2. VERSION NUMBER 1
3. PARTNERED PAVEMENT RESEARCH CENTER STRATEGIC PLAN ELEMENT NUMBER 4.73	4. DRISI TASK NUMBER 3210
5. CALTRANS TECHNICAL LEAD AND REVIEWER(S) Deepak Maskey	6. FHWA NUMBER CA213210B

7. PROPOSALS FOR IMPLEMENTATION
The code for tBeam should be implemented in some form in the pavement life cycle assessment tool eLCAP to provide the capability for analysis of environmental impacts of vehicle propulsion energy dissipation due to the structural response of the pavement under the moving vehicle.

8. RELATED DOCUMENTS
Simulation of Cumulative Annual Impact of Pavement Structural Response on Vehicle Fuel Economy for California Test Sections, UCPRC-RR-2015-05; Investigation of the Effect of Pavement Deflection on Vehicle Fuel Consumption: Field Data Collection, Data Processing and Empirical Analysis, UCPRC-RR-2021-03

9. LABORATORY ACCREDITATION

S. Weissman **FIRST AUTHOR**	J.T. Harvey **TECHNICAL REVIEW**	J.T. Harvey **PRINCIPAL INVESTIGATOR**	D. Maskey **CALTRANS TECH LEAD**	T.J. Holland **CALTRANS CONTRACT MANAGER**

DISCLAIMER

This document is disseminated in the interest of information exchange. The contents of this report reflect the views of the authors who are responsible for the facts and accuracy of the data presented herein. The contents do not necessarily reflect the official views or policies of the State of California or the Federal Highway Administration. This publication does not constitute a standard, specification or regulation. This report does not constitute an endorsement by the California Department of Transportation (Caltrans) of any product described herein.

For individuals with sensory disabilities, this document is available in braille, large print, audiocassette, or compact disc. To obtain a copy of this document in one of these alternate formats, please contact: the California Department of Transportation, Division of Research Innovation, and Systems Information, MS-83, P.O. Box 942873, Sacramento, CA 94273-0001.

For more information:

University of California Pavement Research Center, Davis
One Shields Avenue, Davis, CA 95616

University of California Pavement Research Center, Berkeley
1353 S. 46th St., Bldg. 452, Richmond, CA 94804

www.ucprc.ucdavis.edu

May 10, 2019

tBeam

A Fast Model to Estimate Energy Consumption Due to Pavement Structural Response

Theoretical and Validation Manual

By
Shmuel L. Weissman and James M. Kelly

2901 Benvenue Ave., Berkeley, California 94705
telephone (510) 528-1251 • fax (510) 528-7102 • www.symplectic.com

Table of Contents

Acknowledgments

A University of California Research Agreement #201702289-03 funded this work. We wish to acknowledge the contributions of Drs. Rongzong Wu, Ali Azhar Butt, and John T. Harvey of the University of California Pavement Research Center.

Executive Summary

Improving the sustainability of pavement operations requires that steps be developed to reduce the environmental impact of construction, maintenance, and use of network. An important component of the network's usage is the energy exerted by vehicles. Part of this energy is consumed by losses within the vehicle and due to pavement surface roughness. Another portion is due to structural properties of the pavement itself. Therefore, if the selection of pavement structures is to be guided by sustainability, the influence of the pavement structure on energy consumption should be adequately reflected in the pavement-design decision process.

The energy dissipated in pavements depends on the characteristics of the pavements in general, and on their rate dependence in particular. These properties depend on temperature and "damage." Thus, the energy a traversing vehicle dissipates due to the structure of the pavement depends on the time of day, the season, and the condition (damage) of the pavement. Moreover, the vehicle fleet includes a range of wheel sizes and axle loads. As a result, estimating the lifetime energy dissipated in a pavement structure requires multiple analyses. Specifically, CalME, the pavement design software employed by Caltrans, requires a few thousand such simulations per design, and each project requires the evaluation of a few design alternatives. Therefore, a pavement design process that incorporates sustainability requires the balancing of two opposing needs. The first requirement is the need to obtain a reasonably accurate estimate of the dissipated energy. The second requirement is high numerical efficiency so that incorporating this consideration is feasible.

The tBeam software is designed to meet the above challenges. In particular, tBeam employs a one-dimensional finite-element-based solution of a wheel traveling at a constant velocity on a viscoelastic beam-foundation system. The one-dimensional approach is essential in order to meet the efficiency requirement. Yet, it is not sufficient. Fortunately, a reduction of a few orders of magnitude in the numerical efforts is obtained by formulating the model relative to a moving coordinate system attached to the wheel. Thanks to this strategy it is feasible to employ tBeam for pavement sustainability analysis.

The one-dimensional solution is, by nature, an approximation to the three-dimensional world. This approximation can be improved by incorporating a "correction factor," which is based on comparisons with pavement simulations accounting for the double curvature observed in loaded pavements. In this report, prediction disparity for a single structure is studied. The results show a clear trend where the correction factor decreases with rising temperature and increases with higher velocity. Unfortunately, the present study was insufficient to establish a law for the correction factor, even for the single case studied. The correction factor ranged from about 1.25 at low temperature and high velocity to about 0.6 for high temperature and low velocity.

This report contains three components. The first part presents the underling theory for tBeam, and the details of the implementation. The second part of this report presents closed form solutions for specialized pavement-foundation systems. The third component of the report presents some of the validation simulations undertaken to demonstrate the performance of tBeam, including comparisons with closed form solutions provided in this report. This component also includes comparisons with results obtained for a single viscoelastic plate-foundation system, which are used to develop guidelines for the correction factor noted above.

Finally, this report contains recommendations for further development of tBeam.

1 Introduction

Improving the sustainability of pavement operations requires that steps be developed to reduce the environmental impact of construction, maintenance, and use of the network. An important component of the network's usage is the energy exerted by vehicles. Part of this energy is consumed by losses within the vehicle and due to pavement surface roughness. Another portion is due to structural properties of the pavement itself. Therefore, if the selection of pavement structures is to be guided by sustainability, the influence of the pavement structure on energy consumption should be adequately reflected in the pavement-design decision process.

The energy dissipated in pavements depends on the characteristics of the pavements in general, and on their rate dependence in particular. These properties depend on temperature and "damage." Thus, the energy a traversing vehicle dissipates due to the structure of the pavement depends on the time of day, the season, and the condition (damage) of the pavement. Moreover, the vehicle fleet includes a range of wheel sizes and axle loads. As a result, estimating the lifetime energy dissipated in a pavement structure requires multiple analyses. Specifically, CalME, the pavement design software employed by Caltrans, requires a few thousand such simulations per design, and each project requires the evaluation of a few design alternatives. Therefore, the pavement analysis software must deliver accurate prediction of the dissipated energy while achieving high numerical efficiency.

The UC Davis Pavement Research Center previously undertook a study to estimate the energy dissipated in pavements. This study considered three different simulation approaches:

1. Three-dimensional solid finite element simulations.
2. Axisymmetric hybrid method (finite elements in the axial direction and a series expansion in the radial direction).
3. A load moving on a viscoelastic Euler beam suspended on a Winkler foundation employing the formulation developed in Kelly [1962].

The first approach meets accuracy requirements, but it is far too computationally intensive for the current needs. The second approach is restricted by the axisymmetric assumption, which is not suitable for the problem of a wheel rolling on a pavement. Following Kelly [1962], the third approach offers a highly efficient numerical model that results from formulating the wheel-beam problem relative to an observer attached to the moving wheel. This approach substitutes the time derivative with a spatial derivative (see Section 2), which enables achieving the steady-state solution in one step. Unfortunately, Kelly [1962] (and the implementation noted above) employed the Bernoulli-Euler beam theory that neglects shear deformation, an important deformation mechanism for asphalt-concrete pavements at elevated temperatures. Consequently, simulations may result in poor estimation of the dissipated energy. Thus, all three approaches fall short.

This report provides the theoretical background and validation simulations for the tBeam software that provides a computationally efficient approach for estimating the energy dissipated in pavements traversed by vehicles moving at a constant velocity. In particular, to achieve numerical efficiency, tBeam adopts the beam model viewed by an observer attached to the

moving wheel as proposed by Kelly [1962]. However, tBeam substitutes the shear deformable Timoshenko beam for the Bernoulli-Euler beam employed in option 3 above.

The balance equations for a Timoshenko beam suspended on a viscoelastic Winkler foundation are presented in Section 2. tBeam is finite element based, and the details of this formulation are provided in Section 3. tBeam offer two loading options, which are described in Section 4. Preparing for the validation effort, a number of special-case closed form solutions are presented in Section 5. Next, simulations demonstrating tBeam are provided in Section 6. These simulations include comparison with closed-form solutions and with simulations employing plate elements to represent the beam. Additionally, Section 6 also includes comparisons with simulations where a pavement is modeled as two-dimensional plates on a Winkler foundation. These simulations are used to establish a "correction factor" relating the one-dimensional beam representation to the three-dimensional world. Lastly, concluding remarks, including recommendations for follow-up studies, are offered in Section 7.

2 Timoshenko Beam Resting on a Winkler Foundation

tBeam employs a multilayered linear viscoelastic Timoshenko beam resting on a linear viscoelastic Winkler foundation. This section presents the strong form of the balance of momentum equations. The presentation is confined to the realm of small deformations, and in-plane effects are ignored.

This section is organized as follows. First, Section 2.1 presents the kinematic assumptions for the Timoshenko beam relative to an inertial (fixed) coordinate system. Kelly [1962] proposed an efficient approach to represent the steady-state beam deflections where the formulation is relative to a coordinate system attached to the rolling wheel. Second, the moving coordinate system is introduced in Section 2.2. Third, Section 2.3 presents the formulation for a purely elastic system where the beam model consists of a single layer. Next, in Section 2.4, the model is extended to linear viscoelastic material response (beam and Winkler foundation). Finally, Section 2.5 extends the beam model to include multiple layers.

2.1 Timoshenko Beam Kinematics

The Timoshenko beam (see Timoshenko [1921, 1922]) extends the Bernoulli-Euler beam model (see, *e.g.*, Kelly [1962]), which allows no shear deformation, to permit restricted shear deformation. In particular, the following two assumptions are introduced:

1. A plane normal to the mid-surface in the reference configuration remains a plane, but it is not necessarily normal to the mid surface.
2. The length of a fiber normal to the mid surface remains unchanged throughout the deformation.

These assumptions are expressed in the following restricted displacement field allowed by the Timoshenko beam theory:

$$U_X(X,Y,Z,t) = -Y\varphi(X,t),\ U_Y(X,Y,Z,t) = w(X),\ \text{and}\ U_Z(X,Y,Z,t) = 0. \tag{2.1}$$

In Equations (2.1), the vector (X,Y,Z,t) represents the position of points in the beam relative to an inertial right-handed Cartesian coordinate system, $\boldsymbol{X}$, at time = t. In particular, the coordinate system is chosen so that the X coordinate is aligned with the axial direction of the beam, with the wheel moving in the positive direction; the Y coordinate is in the direction of the normal to the mid-surface, with the origin at the mid-surface and the positive in the upwards direction; and the Z coordinate is normal to both the X and Y coordinates. Also in Equation (2.1), (U_X, U_Y, U_Z) are the components of the displacement vector; $\varphi(X)$ is the angle of rotation about the Z axis of the normal to the mid-surface (it depends only on the X coordinate); and w is the displacement of the mid-surface in the Y-direction, which will henceforward be referred to as the transverse direction. It follows from the above assumptions that the Timoshenko beam model introduces the following shear strain:

$$\gamma(X) \coloneqq \frac{\partial w}{\partial X} - \varphi \tag{2.2}$$

2.2 Moving Coordinate System

Kelly [1962] noticed that an observer attached to a rolling wheel moving at a constant velocity perceives a constant deformation state. This observation led him to formulate the balance of momentum relative to a moving coordinate system, an approach that results in substituting spatial derivative for time derivative. A direct consequence of this approach is that the steady state solution for the entire beam is obtained in one step, thus bypassing the need for time integration and achieving significant computation advantage. Therefore, this approach is implement in tBeam as described below.

Let $\boldsymbol{x}$ denote a second right handed Cartesian coordinate system attached to the rolling wheel so that:

$$x = X - vt,\ y = Y, \text{ and } z = Z. \tag{2.3}$$

In Equations (2.3), v is the velocity of the wheel (assumed to be constant). It follows from the definition of the moving coordinate system that the following relations exist between derivatives:

$$\frac{\partial}{\partial x} = \frac{\partial}{\partial X} \text{ and } \frac{\partial}{\partial t} = \frac{\partial}{\partial x}\frac{\partial x}{\partial t} = -v\frac{\partial}{\partial x}. \tag{2.4}$$

The second of Equations (2.4) provides the means for replacing time derivatives with spatial derivatives. Taking advantage of this relationship enables bypassing time integration altogether (for a steady state analysis), which is pivotal for achieving high numerical efficiency.

2.3 An Elastic Timoshenko Beam on an Elastic Winkler Foundation

The governing equations of motion for an elastic Timoshenko beam on an elastic Winkler foundation, relative to the inertial coordinate system $\boldsymbol{X}$, is given by:

$$\rho A\frac{\partial^2 w}{\partial t^2} - q(X,t) + q^f(x,t) = \frac{\partial Q}{\partial X} \tag{2.5}$$

and

$$\rho I\frac{\partial^2 \varphi}{\partial t^2} = \frac{\partial M}{\partial X} + Q \tag{2.6}$$

In Equations (2.5) and (2.6), ρ is the mass density; A is the area of the cross section of the beam; $w(X,t)$ is the transverse displacement; $q(X,t)$ is a distributed transverse load per unit length; $q^f(X,t)$ is the force exerted on the beam by the Winkler foundation; Q is the shear resultant force; M is the bending moment; and I is the second moment of the Area.

Completing the description requires providing constitutive laws for Q, M, and q^f, which for the case of a linear elastic beam and Winkler foundation are given by:

$$Q = GA_s\gamma,\ M\ = EI\frac{\partial \varphi}{\partial X}, \text{ and } q^f\ = Kw \tag{2.7}$$

In Equations (2.7), G is the shear modulus of the beam; $A_s := kA$ is the effective area of the beam's cross section, with k the Timoshenko shear coefficient, typically for rectangular sections $k = 5/6$; E is the elastic modulus of the beam; and K is the stiffness of the Winkler foundation (per unit length).

Remark: The shear and elastic moduli are related through the following relationship: $G = \frac{E}{2(1+\nu)}$, where ν is Poisson's ratio. It serves the validation effort to keep E and G independent of each other, which will be followed herein. ♦

It was observed in Section 2.2 that enhanced computational efficiency could be attained if the formulation is recast relative to a moving coordinate system attached to the rolling wheel. (A constant velocity is assumed.) Applying Equations (2.4) to Equations (2.5) and (2.6) yields:

$$\rho A v^2 \frac{\partial^2 w}{\partial x^2} - q(x,t) + q^f(x,t) = \frac{\partial Q}{\partial x} \tag{2.8}$$

and

$$\rho v^2 I \frac{\partial^2 \varphi}{\partial x^2} = \frac{\partial M}{\partial x} + Q \tag{2.9}$$

An examination of Equations (2.8) and (2.9) shows that only the inertia terms in both equations changed, introducing the square of the velocity and replacing time derivative with spatial derivative. Additionally, the spatial derivatives are now relative to the moving coordinate system. The constitutive equations (Equations (2.7)) remain unchanged except that the spatial derivatives are relative to the moving coordinate system. This last observation is valid *only* for the rate independent models such as the linear elastic model considered in this section (see Section 2.4).

2.4 A Viscoelastic Timoshenko Beam on a Viscoelastic Winkler Foundation

The purely (linear) elastic model presented in Section 2.3 is now extended linear viscoelasticity. In particular, the Timoshenko beam model consists of three "independent" components: bending, shear, and Winkler foundation. Each of these components is independently replaced with a generalized Maxwell model consisting of the following elements in parallel:

1. A linear "spring" (providing a purely elastic response).
2. A number of linear Maxwell elements (each consisting of a spring in sequence with a dashpot).
3. A linear dashpot.

In a one-dimensional setup, this viscoelastic model is mathematically represented by:

$$\sigma = E\epsilon + \eta \frac{\partial \varepsilon}{\partial t} + \sum_{i=1}^{n} \sigma_i^M \tag{2.10}$$

In Equation (2.10), σ is the stress; E is the stiffness of the elastic spring; ϵ is the (total) axial strain; η is the viscosity of the "stand-alone" dashpot; n is the number of Maxwell elements; and σ_i^M is the stress in the ith Maxwell element, which is given by:

$$\sigma_i^M = E_i(\epsilon - \varepsilon_i^M) = \eta_i \frac{\partial \varepsilon_i^M}{\partial t}. \tag{2.11}$$

In Equation (2.11), E_i and η_i are the "spring" and "dashpot" properties comprising the ith Maxwell element, respectively; ε_i^M is the viscous strain in the ith Maxwell element, which is introduced here as an internal variable. Equation (2.11) reflects the fact that the spring and dashpot are thought of as being in sequence; hence, the stress in them is equal. It is often convenient to work with the characteristic period of the Maxwell element, which is defined by:

$$\tau_i := \frac{\eta_i}{E_i}. \tag{2.12}$$

The representation of the Maxwell elements introduced the internal variables ε_i^M. Thus, in order to proceed, a relation is needed to evaluate the internal variables. The second equality in Equation (2.11) provides the needed relationship, which can be casted as a rate equation for ε_i^M, as follows:

$$\frac{\partial \varepsilon_i^M}{\partial t} = \frac{\epsilon - \varepsilon_i^M}{\tau_i}. \tag{2.13}$$

Equation (2.13) takes advantage of the definition of the characteristic time (Equation (2.12)).

An examination of Equations (2.10) and (2.11) reveals that they contain time derivatives, which in the moving coordinate system, thanks to Equation (2.4), can be expressed in terms of spatial derivatives. Accordingly, Equations (2.10) and (2.11) can be respectively rewritten as:

$$\sigma = E\epsilon - \eta v \frac{\partial \varepsilon}{\partial x} + \sum_{i=1}^{n} \sigma_i^M \tag{2.14}$$

and

$$\sigma_i^M = E_i(\epsilon - \varepsilon_i^M) = -E_i \tau_i v \frac{\partial \varepsilon_i^M}{\partial x}. \tag{2.15}$$

ε_i^M appearing in Equation (2.15) is an internal variable, associated with the ith Maxwell element. Its physical interpretation is the portion of the total strain due to the elongation of the dashpot component of the Maxwell element. In other words, as implicitly stated by Equation (2.15), the total strain admits an additive decomposition into elastic and viscous strains (*i.e.*, $\epsilon = \varepsilon_i^e + \varepsilon_i^M$), and the elastic strain, $\varepsilon_i^e(\epsilon, \epsilon^{e}{}_i^M)$, is taken as the dependent variable. Equation (2.14) also took advantage of the characteristic time, which is defined by Equation (2.12). Finally, the internal variables ε_i^M are determined, in an analogous way to Equation (2.13) through the following relation:

$$\frac{\partial \varepsilon_i^M}{\partial x} = -\frac{\epsilon - \varepsilon_i^M}{\tau_i v}. \tag{2.16}$$

Examining the elastic constitutive laws expressed by Equations (2.7) reveals that all three (bending, shear, and foundation) are essentially one-dimensional laws, and the one-dimensional constitutive model derived in this section is directly applicable with the appropriate strain measure, which for the three cases is given by:

1. Bending: $I\frac{\partial \varphi}{\partial x}$.
2. Shear: $A_s\gamma$.
3. Winkler foundation: w.

For example, the constitutive equation for bending, in the inertial coordinate system, is given by:

$$M = EI\frac{\partial \varphi}{\partial x} + \eta I\frac{\partial^2 \varphi}{\partial t \partial x} + \sum_{i=1}^{n} E_i I\left(\frac{\partial \varphi}{\partial x} - \kappa_i^M\right). \tag{2.17}$$

Alternatively, in the moving coordinate system, it is given by:

$$M = EI\frac{\partial \varphi}{\partial x} - v\eta I\frac{\partial^2 \varphi}{\partial x^2} + I\sum_{i=1}^{n} E_i\frac{\partial \kappa_i^M}{\partial x}\left(\frac{\partial \varphi}{\partial x} - \kappa_i^M\right). \tag{2.18}$$

In Equations (2.17) and (2.18), κ_i^M is the internal variable associated with the i[th] Maxwell element. The last term in Equation (2.18) retains the form used in Equation (2.17) rather than the alternative form for the constitutive form on the Maxwell element (*i.e.*, in terms of the stress on the dashpot). This choice is made because the internal variable is directly accessible, and using this form avoids introducing higher derivatives.

2.5 A Multilayered Viscoelastic Timoshenko Beam on a Viscoelastic Winkler Foundation

The balance equations, for a multilayered beam resting on a Winkler foundation, relative to the inertial coordinate system $\boldsymbol{X}$, are given by:

$$\frac{\partial^2 w}{\partial t^2}\sum_{n=1}^{nL}(\rho A)_n - q(X,t) + q^f(x,t) = \frac{\partial Q}{\partial X} \tag{2.19}$$

and

$$\frac{\partial^2 \varphi}{\partial t^2}\sum_{n=1}^{nL}(\rho I)_n = \frac{\partial M}{\partial X} + Q \tag{2.20}$$

In Equations (2.19) and (2.20), nL represents the number of layers comprising the beam, and ρ_n, A_n, and I_n are the mass density, area, and second area moment for the n[th] layer, respectively.

tBeam is formulated relative to a moving coordinate system, $\boldsymbol{x}$, moving at a constant velocity v. In this moving coordinate system, the balance equations are given by:

$$v^2\frac{\partial^2 w}{\partial x^2}\sum_{n=1}^{nL}(\rho A)_n - q(x,t) + q^f(x,t) = \frac{\partial Q}{\partial x} \tag{2.21}$$

and

$$v^2 \frac{\partial^2 \varphi}{\partial x^2} \sum_{n=1}^{nL} (\rho I)_n = \frac{\partial M}{\partial x} + Q \tag{2.22}$$

The resultants M, Q, and q^f, relative to the inertial coordinate system $\boldsymbol{X}$, are respectively given by:

$$M = \sum_{n=1}^{nL} \left(EI \frac{\partial \varphi}{\partial x} + \eta^B I \frac{\partial^2 \varphi}{\partial t \partial x} \right)_n + \sum_{n=1}^{nL} \left(I_n \sum_{i=1}^{nB,n} E_{ni} \left(\frac{\partial \varphi}{\partial x} - \kappa_{ni}^M \right) \right), \tag{2.23}$$

$$Q = \sum_{n=1}^{nL} \left(GA_s \gamma + \eta^S A_s \frac{\partial \gamma}{\partial t} \right)_n + \sum_{n=1}^{nL} \left(A_{s_n} \sum_{i=1}^{nS,n} G_{ni} (\gamma - \gamma_{ni}^M) \right), \tag{2.24}$$

and

$$q^f = Kw + \eta^f \frac{\partial w}{\partial t} + \sum_{i=1}^{nF} K_i^M (w - w_i^M). \tag{2.25}$$

In Equations (2.23) to (2.25), nB,n and nS,n are the numbers of bending and shear Maxwell elements for the nth layer; nF is the number of Maxwell elements used for the foundation; $(EI)_n$ is the product of the modulus and second moment of the area for the nth layer (stand-alone spring); $(\eta^B I)_n$ is the product of the bending-viscosity and second moment of the area for the nth layer (stand-alone dashpot); E_{ni} is the modulus associated with the ith bending Maxwell element of the nth layer; κ_{ni}^M is the internal variable corresponding to the ith bending Maxwell element of the nth layer; $(GA_s)_n$ is the product of the shear modulus and effective area for the nth layer (stand-alone spring); $(\eta^S I)_n$ is the product of the shear-viscosity and second moment of the area for the nth layer (stand-alone dashpot); G_{ni} is the shear modulus associated with the ith shear Maxwell element of the nth layer; γ_{ni}^M is the internal variable corresponding to the ith shear Maxwell element of the nth layer; K is the elastic stiffness of the foundation (stand-alone spring); η^f is the viscosity of the foundation stand-alone dashpot; K_i^M is the stiffness of the ith foundation Maxwell element; and w_i^M is the internal variable associated with the ith foundation Maxwell element.

The constitutive Equations (2.23) through (2.25) are relative to the inertial coordinate system $\boldsymbol{X}$. Their counterparts relative to a moving coordinate system, $\boldsymbol{x}$, moving at a constant velocity v are given by:

$$M = \sum_{n=1}^{nL} \left(EI \frac{\partial \varphi}{\partial x} - v \eta^B I \frac{\partial^2 \varphi}{\partial x^2} \right)_n - v \sum_{n=1}^{nL} \left(I \sum_{i=1}^{nB,n} \left(\eta^{BM} \frac{\partial \kappa^M}{\partial x} \right)_i \right)_n, \tag{2.26}$$

$$Q = \sum_{n=1}^{nL} \left(GA_s \gamma - v \eta^S A_s \frac{\partial \gamma}{\partial x} \right)_n - v \sum_{n=1}^{nL} \left(A_{s_n} \sum_{i=1}^{nS,n} \left(\eta^{SM} \frac{\partial \gamma^M}{\partial x} \right)_i \right)_n, \tag{2.27}$$

and

$$q^f = Kw - v \eta^f \frac{\partial w}{\partial x} - v \sum_{i=1}^{nF} \left(\eta^{fM} \frac{\partial w^M}{\partial x} \right)_i. \tag{2.28}$$

The last term in each of Equations (2.26) through (2.28) is associated with the Maxwell elements of the bending, shear, and foundation, respectively. The representation is in terms of the stress acting on the respective dashpots, which in the inertial coordinate system is expressed in terms of the strain rate and in the moving coordinate system in terms of the velocity and the spatial derivative, as desired for the approach pursued in tBeam.

3 The Weak Form of the Timoshenko Beam on Winkler Foundation Equations and Their Finite Element Approximation

tBeam is finite element based. Accordingly, it is derived from the weak form of the momentum equations, where the equations are enforced only in an integral sense relative to weight functions (see, *e.g.*, Hughes [1987]). The weak form is presented in Section 3.1. Details of the finite element approximation are provided in Section 3.2. tBeam employs a Gaussian quadrature to integrate the balance of momentum equations, a topic covered in Section 3.3. Finally, addressing internal variables in a moving coordinate system is presented in Section 3.4.

3.1 The Weak Form

The strong form (*i.e.*, enforced point wise) of the balance of momentum equations for a Timoshenko beam on a Winkler foundation is presented in Section 2. The weak form counterpart (*i.e.*, enforced only in an integral sense) that constitutes the basis for the finite element approximation employed in tBeam is presented herein. Specifically, the weak counterpart to Equations (2.19) and (2.20), the balance equations in the moving coordinate system, are, respectively, given by:

$$\int \theta_w \left(v^2 \frac{\partial^2 w}{\partial x^2} \sum_{n=1}^{nL} (\rho A)_n - q(x,t) + q^f(x,t) - \frac{\partial Q}{\partial x} \right) dx = 0 \tag{3.1}$$

and

$$\int \theta_\varphi \left(v^2 \frac{\partial^2 \varphi}{\partial x^2} \sum_{n=1}^{nL} (\rho I)_n - \frac{\partial M}{\partial x} - Q \right) dx = 0 \tag{3.2}$$

The integrals appearing in Equations (3.1) and (3.2) are over the domain of the beam. Additionally, θ_w, and θ_φ appearing in Equation (3.1) and (3.2) are weight functions, or variations, representing allowable transverse displacement (θ_w) and rotations (θ_φ), such that they vanish at the end points.

An examination of the constitutive laws for the moment, M, and shear, Q, resultants shows that they include spatial derivatives of the transverse displacement, w, and rotation, φ, respectively. Therefore, in order to reduce continuity requirements on the space of admissible displacements (w, φ), Equations (3.1) and (3.2) are integrated by parts as follows:

$$\int \frac{\partial \theta_w}{\partial x} \left(Q - v^2 \frac{\partial w}{\partial x} \sum_{n=1}^{nL} (\rho A)_n \right) dx + \int \theta_w \left(q^f(x,t) - q(x,t) \right) dx = 0 \tag{3.3}$$

and

$$\int \frac{\partial \theta_\varphi}{\partial x} \left(M - v^2 \frac{\partial \varphi}{\partial x} \sum_{n=1}^{nL} (\rho I)_n \right) dx - \int \theta_\varphi (Q) dx = 0 \tag{3.4}$$

3.2 The Finite Element Approximation

The finite element approximation of Equations (3.3) and (3.4) is obtained by introducing base functions. The geometry and state variables (*e.g.*, displacement, velocity, and acceleration) are approximated by:

$$y = N_I Y_I \tag{3.5}$$

In Equation (3.5), y represents any interpolated quantity (*e.g.*, displacement); N_I is the shape function associated with the I^{th} node; Y_I is the value of the interpolated quantity evaluated at node I; and summation over I is implied. Employing the same approximation for the geometry and state variables is termed isoparametric formulation.

tBeam employs three-node beam elements, whose shape functions are given by:

$$N_1 = \frac{1}{2}\xi(\xi - 1),\ N_2 = 1 - \xi^2,\ \text{and}\ N_3 = \frac{1}{2}\xi(\xi + 1). \tag{3.6}$$

In Equations (3.6), $\xi \in [-1,1]$ is the element's natural coordinate, and the N1, N2, and N3 nodes' natural coordinates are $-1,\ 0,$ and 1, respectively. Figure 3.1 depicts the three shape functions versus the natural coordinate. Note that although the nodes are equally spaced in the natural space, they need not be so in the physical space. The only restriction is that the middle node is between the two end nodes. A common restriction on the shape functions is that they obey the partition of unity (*i.e.*, summation of the values of the shape functions at any point within the element domain is one). A simple verification shows that indeed the three shape functions sum to one at every point within the element.

Figure 3.1: Shape functions.

The momentum equations and constitutive laws employ spatial derivations, which in the finite element context are given by:

$$\frac{\partial y}{\partial x} = \frac{\partial N_I}{\partial x} Y_I = \frac{\partial N_I}{\partial \xi}\frac{\partial \xi}{\partial x} Y_I \tag{3.7}$$

The last expression in Equation (3.7) includes $\frac{\partial \xi}{\partial x}$, introduced by the chain rule.

The finite element approximation commences with the division of the domain into non-overlapping subdomains, whose union is an approximation of the total domain. (The approximation is exact for the one-dimensional case considered here.) Within each subdomain, termed element, the balance of momentum equations are applied, with the geometry and state variables approximated by Equation (3.5). (The use of the same shape functions for the geometry and weight functions, θ_w and θ_φ, is termed the Bobnov-Galerkin approach (see, *e.g.*, Hughes [1987])). By introducing the approximation, the problem is converted from solving differential equations to solving algebraic equations, which are obtained by assembling the element arrays. Details of the finite element assembly process can be found in finite element textbooks (see, *e.g.*, Hughes [1987]).

3.3 Numerical Integration

The weak form of the balance of momentum equations requires integration. tBeam employs a Gaussian quadrature approximation (see, *e.g.*, Hughes [1987]), given by:

$$\int_a^b F(x)dx = \int_{-1}^{1} F(x)\frac{\partial x}{\partial \xi}d\xi \approx \sum_{I=1}^{n}\left(WF\frac{\partial x}{\partial \xi}\right)_I \tag{3.8}$$

In Equation (3.8), $F(x)$ is a function defined over the interval $x \in [a,b]$; n is the number of integration points; W_I are integration weights obeying the restriction: $\sum_{I=1}^{n} W_I = 2$; and $\frac{\partial x}{\partial \xi}$ is the Jacobian of the transformation (physical to natural coordinates).

Remark: Recall that the element's natural space is also defined on the interval $\xi \in [-1,1]$. This choice is intentional. It is made in order to facilitate Gaussian quadrature. ♦

As noted in Section 3.2, tBeam employs quadratic shape functions. Conventionally, when employing quadratic shape function, the balance equations are integrated using a three-point quadrature, also referred to as full integration for this case. Unfortunately, for the Timoshenko beam, employing full integration gives rise to shear locking, where energy is diverted from bending to shear modes. This problem arises in modeling thin beams, and it is manifested by the need to use very fine meshes to obtain converged solutions (see *e.g.*, Hughes [1987]). A simple remedy to this problem is the use of selective reduced integration where the bending terms are integrated using a three-point quadrature, and the shear terms are integrated using a two-point quadrature (see *e.g.*, Hughes [1987]). The weights and natural coordinates of the integration points are summarized in Table 3.1.

Table 3:1 Gaussian Quadrature: location and weights.

Point #	2-point		3-point	
	ξ	W	ξ	W
1	$-\sqrt{3}/3$	1.0	$-\sqrt{0.6}$	$5/9$
2	$\sqrt{3}/3$	1.0	0	$8/9$
3			$\sqrt{0.6}$	$5/9$

3.4 Maxwell Elements in Moving Coordinate Systems

The generalized Maxwell element constitutive model employed in tBeam (see Equations (2.26) through (2.28)) employs internal variables, one per each Maxwell element. When the representation is relative to an inertial coordinate system, the rate equation used to update internal variables can be numerically integrated in time using methods such as the backward Euler scheme (see, *e.g.*, Hughes [1987]). Finite element approximations accommodate internal variables by storing history terms at integration (Gauss) point and updating them using rate equations such as Equation (2.13).

tBeam is formulated relative to a moving coordinate system. As shown Section 2, this transformation avoids the need for time integration, which facilitates a very efficient numerical analysis. However, by removing the time dimension it also renders the history-variables strategy unusable. It is instructive to examine rate equation (2.16), rate Equation (2.13) transformed to the moving coordinate system, which after rearranging takes the following form:

$$\varepsilon^M - \tau v \frac{\partial \varepsilon^M}{\partial x} = \epsilon. \tag{3.9}$$

Equation (3.9) addresses a generic Maxwell element, and so the sub-index, designating the Maxwell element number, was removed. Introducing the first-order approximation for the spatial derivative, the analog to the Backward Euler scheme in time, Equation (3.9) can be approximated by:

$$\varepsilon_z^M - \tau v \frac{\varepsilon_{z+\Delta L}^M - \varepsilon_z^M}{\Delta L} = \epsilon_z. \tag{3.10}$$

In Equation (3.10) the subscript designate the point along the beam the rate equation is applied, and ΔL is a length increment. After further regrouping, the following update formula for the internal variable is arrived at:

$$\varepsilon_z^M = \frac{\tau v \varepsilon_{z+\Delta L}^M + \Delta L \epsilon_z}{\tau v + \Delta L}. \tag{3.11}$$

Equation (3.11) reveals that, in the moving coordinate system, the history for the internal variables is found downstream (*i.e.*, in the direction the wheel is moving in). This observation can be understood on physical grounds as follows. The state at the current point z Δt time ago, is the same as the current state at the point located at $z + v\Delta t$. In other words, looking back in time the inertial coordinate system is replaced, in the moving coordinate system, by looking downstream.

Equation (3.11) provides insights into the algorithmic approach pursued when the equations of motion are viewed from the perspective of an observer attached to the moving wheel. A closer examination shows that it corresponds to applying the finite element spatial approximation to Equation (3.9) in the case of a (linear) two-node element, where ΔL is the length of the element. In other words, the look downstream approach naturally presents itself when the finite element spatial approximation is applied to Equation (3.9).

The tBeam implementation takes the "looking downstream" approach to the three-node Timoshenko beam element. The implementation introduces a global degree-of-freedom for each Maxwell element, and enforces the finite element approximation to Equation (3.9) at the two upstream nodes (*i.e.*, the nodes closer to where the wheel comes from; in the tBeam implementation these are the two nodes with the smaller x-coordinate values; velocity is assumed to be positive). This equation is given by:

$$N_I \varepsilon_I^M - \tau v \frac{\partial N_I}{\partial x} \varepsilon_I^M = N_I \epsilon_I. \tag{3.12}$$

(Recall that repeated indices imply summation; in this case, over the three nodes.) The tBeam implementation makes the values of the internal variable at the two upstream nodes depend on the total strain and on the value of the internal variable at the downstream node, a restriction that is added as an explicit equation to the global stiffness matrix. As long as the element considered has a downstream neighbor, this approach works. The next element will express the internal variable at its upstream node, which is shared with its upstream neighboring element, to the total strain and the internal variable at its downstream most node. This process breaks down when it comes to the last element in the downstream direction, which is left without any "stiffness" for the added degree-of-freedom at the last node! Fortunately, if the last downstream node is taken far enough ahead of the load, the internal variable there is not affected by the load; it can be fixed as a boundary condition, and the value set to zero. Thus, for the tBeam results to be accurate, the last downstream node must be at a sufficient distance ahead of the load to justify this assumption.

Remarks:

1. In the tBeam implementation, the mesh is constructed to be symmetric about the location of the wheel (taken to coincide with $x = 0$), and the length in each direction is user defined. tBeam also automatically fixes all the degrees-of-freedom added for the internal variables at the downstream most node. A consequence of this implementation is that tBeam requires that the velocity be greater than zero.
2. The strategy adopted for tBeam of adding degrees-of-freedom creates an implicit dependency that renders the internal variable at a given node dependent on what its value is downstream. It is possible, albeit very cumbersome, to avoid adding the degrees-of-freedom and constructing an explicit dependency on the values of the internal variables at all nodes downstream of the node under consideration. Such an implementation would reduce, potentially significantly, the number of equations solved. However, the reduced system will be both complex to construct and result in a full stiffness matrix, which would considerably slow down the solution. Given that tBeam employs a one-dimensional model, it was judged that adopting the strategy of adding degrees-of-freedom leads to superior numerical efficiency. ♦

4 Analysis Options

tBeam can be used to determine the deflection bowl and dissipated energy for multilayer viscoelastic Timoshenko beams resting on viscoelastic Winkler foundations. Two types of loadings can be applied. Under the first option, a uniformly distributed force per unit length is applied as described in Section 4.1. The second option, discussed in Section 4.2, considers a vertical force applied to a rolling rigid wheel.

4.1 Uniformly Distributed Force Per Unit Length

Applying a uniformly distributed force per unit length to a segment at the center of the beam is the simpler of the two solution strategies supported by tBeam. The user specifies the length, magnitude, and (constant) velocity of the force. The force is applied to the center of the beam's finite element model, and a profile solver is applied to solve the linear system of equation resulting from the assembly of the element stiffness matrices and right-hand-side (load) vector (see, *e.g.*, Taylor [1985]).

4.2 Rolling Rigid Wheel

tBeam offers the ability to simulate the response of pavements to rolling rigid wheels of (user-specified) radius, R, subjected to a user-specified vertical force, F_{ext}. In this case, the task is complicated by the fact that the tire-pavement contact zone depends on properties of the system (*e.g.*, velocity, R, F_{ext}, and material properties), which requires the solution of a two-body contact problem.

tBeam is set up within the realm of small deformations, which permits the use of a node-on-node contact algorithm. This contact resolution strategy is discussed in Section 4.2.1. The basic step within this strategy consists of imposing the vertical position of the wheel (*i.e.*, how far it moved down) and determining the applied nodal forces required to prevent penetration. The sum of these forces (*i.e.*, the force transmitted from the wheel to the pavement) will not, in general, equal the externally applied load. The strategy employed in tBeam to position the wheel so that the contact force equals the external force is described in Section 4.2.2. Finally, Section 4.2.3 provides the details of how the wheel-pavement contact is implemented in tBeam.

4.2.1 Node-on-Node Contact Strategy

tBeam is setup within the realm of small deformations, which permits the use of a node-on-node contact algorithm (see, *e.g.*, Hughes *et al*. [1976]). The underlying idea of this approach is that nodes on the surface of body A are paired with nodes on the surface of body B. Each node-pair is connected with a node-on-node contact element. The contact elements are stiff springs that are activated when the dot product of the vector from node A to node B with a specified vector (vertical in tBeam) changes sign. Otherwise, the spring remains inactive (*i.e.*, no contact force is applied between the two nodes). When penetration is detected, the forces exerted by the springs act to reduce the penetration. This problem is nonlinear, and requires an iterative solution strategy. tBeam employs a Newton iteration. Thus, this solution strategy is more computationally intensive than that required to solve for the loading described in Section 4.1, which requires only

one solution of the system of algebraic equations generated by the finite element model. (A profile solver is used to solve the system of equations (see, *e.g.*, Taylor [1985]).)

Remark: The solution strategy described above is known as a penalty method. In theory, the higher the value assigned to the stiffness of the node-on-node contact elements, the better the no-penetration constraint is enforced. In practice, however, assigning a stiffness that is too large may cause numerical problems because it results in a stiff system of equations (*i.e.*, large ratio between the eigenvalues of the stiffness matrix). Conversely, choosing a value that is too low results in excessive penetration. The general guideline, for contact of two elastic bodies, is to choose a stiffness that is of the order of the elastic moduli of the bodies. In tBeam, one of the bodies (the wheel) is rigid, so the relevant moduli is that of the pavement. However, the pavement is not elastic, and some judgment should be used. In the examples provided in Section 6, values ranging from 10 to 100 times the effective stiffness were used. ♦

As noted above, node-on-node contact elements introduce stiff "springs" between the pairs of nodes. These springs require a law relating the penetration to the force applied to counter it. tBeam employs the following nonlinear force-penetration law:

$$f = K\left(\frac{\epsilon}{L_{ref}}\right)^{p-1}. \tag{4.1}$$

In Equation (4.1), f is the force applied to counter the penetration; K is a user specified stiffness value; L_{ref} is a user specified reference length[1]; p is a user specified power; and ϵ is the "length" of the penetration. The examples in Section 6 employ $p = 2$, which leads to a linear force-penetration law.

4.2.2 Determining the Vertical Position of the Rigid Wheel

The description thus far explained the setting of the contact problem. To determine the penetration requires knowing the vertical position of the wheel, which is unknown. What is known is the force applied to the wheel and the wheel's radius. Determining the vertical position of the rigid wheel requires enforcing the following identity:

$$F_{int}^{n}(w_{rw}^{n}) = F_{ext}. \tag{4.2}$$

In Equation (4.2), F_{int}^{n} is the sum of the forces in the all contact elements in the n[th] iteration[2] (when the wheel center is positioned at $(0, R - w_{rw}^{n})$); w_{rw}^{n} is the distance the wheel moved down; and F_{ext} is the external vertical force applied to the wheel. Using a Newton iteration to solve Equation (4.2) leads to:

$$F_{int}^{n}(w_{rw}^{n}) + K^{n}\Delta w_{rw}^{n} = F_{ext}. \tag{4.3}$$

[1] For tBeam, it is recommended that L_{ref} be taken as the length of the beam elements connected to the node on the pavement side of the contact problem.

[2] The iteration is associated with the solution of Equation (4.1). Each such iteration requires the iterative contact resolution iteration discussed above, which is the iteration within the global iteration.

In Equation (4.3), K^n is the tangent stiffness, defined below, and Δw_{rw}^n is the increment in the vertical position of the rigid wheel. A closed form solution to determine K^n is not readily available. Therefore, tBeam resorts to approximating it numerically. To this end, the wheel is first position at $(0, w_{rw}^n - \delta)$, and the contact problem is solved to obtain $F_{int}^n(w_{rw}^n - \delta)$. Here δ is a small (positive) increment automatically set by tBeam. Note that this solution requires a number of iterations. Next, the wheel is repositioned to $(0, w_{rw}^n)$, and $F_{int}^n(w_{rw}^n)$ is obtained, again requiring a number of finite element solutions. The stiffness, K^n, is then approximated by:

$$K^n \approx \frac{F_{int}^n(w_{rw}^n - \delta) - F_{int}^n(w_{rw}^n)}{\delta}. \tag{4.4}$$

The increment in the vertical position of the rigid wheel is given by:

$$\Delta w_{rw}^n = (K^n)^{-1}\left(F_{ext} - F_{int}^n(w_{rw}^n)\right). \tag{4.5}$$

Note that each formation of K^n requires performing the finite element analysis a number of times, consequently making this type of analysis considerably more computationally intensive than analyzing the loading described in Section 4.1.

4.2.3 tBeam Implementation

The solution in tBeam begins by setting up nodes on the bottom half of the circumference of the wheel.[3] The wheel is position so that its center is located at $(0, R)$.[4] The wheel's nodes are positions so that they are directly above beam nodes, and all their degrees-of-freedom are fixed. Next, following the contact approach prescribed above, the corresponding nodes are connected with node-on-node contact elements. These node-on-node contact elements are activated only when the current y-coordinate of the rigid-wheel node falls bellow that of the corresponding beam node (indicating that the rigid wheel penetrated the pavement). When the rigid-wheel node remains above the beam node, no penetration takes place, and the force in the node-on-node contact element is set to zero.

Finally, the above iterative solution for Equation (4.3) requires a starting point. The closer the initial guess of w_{rw}^0 is to the final value, the less iterations are required. Thus, a good strategy to guess the value of w_{rw}^0 is needed. In tBeam, the initial guess is obtained by applying F_{ext} as a point load at $x = 0$. However, if a previous solution was performed (*i.e.*, a different case was studied using the same beam), than the last solution is taken as the initial solution. This approach saves a few iterations, thus reducing the computational effort in solving subsequent cases. Since CalME is expected to run a few thousand simulations for the pavement, the gain is not insignificant relative to the overall analysis time.

[3] The upper part of the rigid wheel need not be represented as they face away from the pavement, which precludes the possibility of them being in contact with the pavement.

[4] Recall that the tBeam solution is relative to a moving coordinate system, where the wheel is always positioned at $x = 0$.

5 Closed Form Solutions of Single-Layered Timoshenko Beam Resting on Winkler Foundation

As part of the tBeam validation effort, presented in Section 6, predicted results are compared with closed-form solutions for a single-layered Timoshenko beam resting on a Winkler foundation. In this section, a number of different combinations of material models for the beam and foundation are examined, and closed-form solutions are developed. For some of the solutions, expressions are developed for the horizontal force needed to sustain the forward motion of the wheel at the specified (constant) velocity. The ratio of the horizontal force to the applied vertical force is defined as a rolling friction coefficient.

An elastic beam-foundation system is considered in Section 5.1. A rigid wheel moving at a constant velocity loads the beam. There is no dissipation in this case, yet the solution is complex. To simplify the solution, the case where the beam is rigid in bending (*i.e.*, $EI \to \infty$) is considered in Section 5.2. Henceforward, this special beam is referred to as a shear beam. tBeam is developed to enable efficient predictions of energy dissipated in the pavement structure. Exploration of this aspect begins in Section 5.3 where the elastic foundation material employed in Section 5.2 is replaced with a Kelvin-Voigt linear viscoelastic material. Next, in Section 5.4, the Kelvin-Voigt foundation is replaced with a Maxwell foundation. Viscoelasticity of the beam is introduced in Section 5.5, where the elastic shear model is replaced with a Maxwell linear viscoelastic response, sharing the same characteristic period as the foundation. Finally Section 5.6 provides the solution of a viscoelastic (Maxwell) beam-foundation system subjected to a uniformly distributed pressure.

5.1 Elastic Beam on Elastic Foundation; Roller Indentation

The pair of second order balance equations governing the Timoshenko beam resting on a Winkler foundation, Equations (2.5) and (2.6), can be replaced by a single fourth order equation. For the case of a linear elastic beam, the governing equation, in the moving coordinate system and ignoring inertia, is given by:

$$\frac{\partial^4 w(x)}{\partial x^4} = \frac{1}{EI} p - \frac{1}{GA_S} \frac{\partial^2 p}{\partial x^2}. \tag{5.1}$$

An elastic foundation is incorporated into the system by replacing p by $p - Kw$, which leads to:

$$\frac{\partial^4 w}{\partial x^4} = \frac{1}{EI} (p - Kw) - \frac{1}{GA_S} \frac{\partial^2 (p - Kw)}{\partial x^2}. \tag{5.2}$$

Regrouping terms in Equation (5.2) leads to:

$$EI \frac{\partial^4 w}{\partial x^4} - \frac{EI}{GA_S} K \frac{\partial^2 w}{\partial x^2} + Kw = p - \frac{EI}{GA_S} \frac{\partial^2 p}{\partial x^2}. \tag{5.3}$$

When the elastic beam-foundation is subjected to a rolling rigid wheel at $x = 0$, the contact area and deformation pattern are symmetric about the origin. Let the closed interval $x \in [-a, a]$ designate the contact area, and Δ designate the indentation. In this case, in the contact area the transverse displacement, $w(x)$, satisfies the following restrictions:

$$w(x) = \frac{x^2}{2R} - \Delta, \frac{\partial w(x)}{\partial x} = \frac{x}{R}, \text{ and } \frac{\partial^2 w(x)}{\partial x^2} = \frac{1}{R} \tag{5.4}$$

Outside the contact area, $p = 0$, so that Equation (5.3) is reduced to:

$$EI\frac{\partial^4 w}{\partial x^4} - \frac{EI}{GA_s}K\frac{\partial^2 w}{\partial x^2} + Kw = 0. \tag{5.5}$$

Let $\alpha^2 \coloneqq \frac{K}{GA_s}$ and $\beta^4 \coloneqq \frac{K}{EI}$. Substituting these definitions into Equation (5.5) leads to:

$$\frac{\partial^4 w(x)}{\partial x^4} - \alpha^2\frac{\partial^2 w}{\partial x^2} + \beta^4 w = 0. \tag{5.6}$$

Equation (5.6) is a homogenous fourth order differential equation whose solution takes the form $w(x) = e^{\lambda x}$. Thus, finding a solution to Equation (5.6), outside the contact zone, is reduced to solving the following fourth-order characteristic polynomial:

$$\lambda^4 - \alpha^2\lambda^2 + \beta^4 = 0. \tag{5.7}$$

The solution of Equation (5.7) is given by:

$$\lambda^2 = \frac{\alpha^2}{2}\left(1 \pm \sqrt{1 - \frac{4\beta^4}{\alpha^4}}\right). \tag{5.8}$$

It follows from Equation (5.8) that the solution depends on the magnitude of the quotient:

$$\frac{4\beta^4}{\alpha^4} = \frac{4K}{EI}\left(\frac{GA_S}{K}\right)^2 = \frac{(2GA_S)^2}{KEI} \tag{5.9}$$

In particular the following three solution types are possible:

Case (i): beam strong in shear

This case corresponds to $\frac{(2GA_S)^2}{KEI} > 1$, which leads to:

$$\lambda^2 = \frac{\alpha^2}{2}\left(1 \pm i\sqrt{\frac{4\beta^4}{\alpha^4} - 1}\right). \tag{5.10}$$

Thus, the four roots are given by:

$$\begin{aligned}
\lambda_1 &= \frac{\alpha}{\sqrt{2}}\rho^{\frac{1}{2}}e^{i\vartheta/2} = \alpha_1 + i\beta_1 \\
\lambda_2 &= \frac{\alpha}{\sqrt{2}}\rho^{\frac{1}{2}}e^{-i\vartheta/2} = \alpha_1 - i\beta_1 \\
\lambda_3 &= \frac{\alpha}{\sqrt{2}}\rho^{\frac{1}{2}}e^{i(\pi-\vartheta)/2} = -\alpha_1 + i\beta_1 \\
\lambda_3 &= \frac{\alpha}{\sqrt{2}}\rho^{\frac{1}{2}}e^{-i(\pi-\vartheta)/2} = -\alpha_1 - i\beta_1
\end{aligned}. \tag{5.11}$$

The transverse displacement is given by:

$$w(x) = Ae^{\alpha_1 x}cos(\beta_1 x) + Be^{\alpha_1 x}sin(\beta_1 x) + Ce^{-\alpha_1 x}cos(\beta_1 x) + De^{-\alpha_1 x}sin(\beta_1 x). \tag{5.12}$$

In Equation (5.12) A, B, C, and D are constants to be determined.

Case (ii): beam weak in shear

The second possible solution occurs when $\frac{(2GA_S)^2}{KEI} < 1$. This is the case of a beam weak in shear. In this case, the two solutions for λ^2 are both positive, resulting in four real roots:

$$\begin{aligned}
\lambda_1 &= \frac{\alpha}{\sqrt{2}}\left(1+\left(1-\frac{4\beta^4}{\alpha^4}\right)^{\frac{1}{2}}\right)^{\frac{1}{2}} =: \alpha_2 \\
\lambda_2 &= -\frac{\alpha}{\sqrt{2}}\left(1+\left(1-\frac{4\beta^4}{\alpha^4}\right)^{\frac{1}{2}}\right)^{\frac{1}{2}} =: -\alpha_2 \\
\lambda_3 &= \frac{\alpha}{\sqrt{2}}\left(1-\left(1-\frac{4\beta^4}{\alpha^4}\right)^{\frac{1}{2}}\right)^{\frac{1}{2}} =: \beta_2 \\
\lambda_3 &= -\frac{\alpha}{\sqrt{2}}\left(1-\left(1-\frac{4\beta^4}{\alpha^4}\right)^{\frac{1}{2}}\right)^{\frac{1}{2}} =: -\beta_2
\end{aligned}, \tag{5.13}$$

and the transverse displacement is given by:

$$w(X) = Ae^{\alpha_2 x} + Be^{-\alpha_2 x} + Ce^{\beta_2 x} + De^{-\beta_2 x}. \tag{5.14}$$

Case (iii): $\frac{(2GA_S)^2}{KEI} = 0$.

In this case, the roots are $\lambda = \pm\frac{\alpha}{\sqrt{2}}$, each repeated twice. The transverse displacement is given by:

$$w(x) = Ae^{\frac{\alpha x}{\sqrt{2}}} + BXe^{\frac{\alpha x}{\sqrt{2}}} + Ce^{\frac{-\alpha x}{\sqrt{2}}} + DXe^{\frac{-\alpha x}{\sqrt{2}}}. \tag{5.15}$$

In the contact region, $x \in [-a, a]$, in view of Equation (5.4), the balance of momentum, Equation (5.3), is reduced to:

$$K\left(\frac{x^2}{R} - \Delta\right) - \frac{EI}{GA_S}\frac{K}{R} = p - \frac{EI}{GA_S}\frac{\partial^2 p}{\partial x^2}. \tag{5.16}$$

Let $\gamma_1^2 := \frac{GA_S}{EI}$. Substituting γ_1^2 into Equation (5.16) results in:

$$\frac{\partial^2 p}{\partial x^2} - p = \frac{K}{R} - \gamma_1^2 K\left(\frac{x^2}{R} - \Delta\right). \tag{5.17}$$

The complementary solution to equation (5.17), in the interval $x \in [-a, a]$, is given by:

$$p(x) = Ecosh(\gamma_1 x) + Fsinh(\gamma_1 x). \tag{5.18}$$

In Equation (5.18), E and F are constants to be determined. The particular solution to Equation (5.17) is given by:

$$p(X) = -K\Delta + \frac{Kx^2}{2R}. \tag{5.19}$$

The above solution expresses the contact zone $x \in [-a, a]$ in terms of the indentation Δ. Once the contact zone is known, the next step is to determine the pressure distribution in the contact zone, noting that the pressure distribution, for the elastic case, is symmetric about the origin. Once the contact pressure, $p(x)$, is determined, it can be integrated to obtain the applied force required to impose the prescribed indentation, Δ.

Thanks to the symmetry of the solution about the origin, for a prescribed Δ, the task at hand consists of the following three steps:

1. Compute the contact half-length, a.
2. Determine the pressure distribution in the contact area.
3. Integrate the contact pressure to determine the applied load F_{ext}.

Taking advantage of the symmetry of the solution, for each of the three types of beam identified above, there are four unknowns: the contact length, a; two constants in the solution of w; and one constant in the solution of p. These four unknowns are determined by imposing continuity conditions across the interface at $x = a$.

The first step towards developing the required continuity equations is to integrate both sides of Equation (5.3) from $x = a - \varepsilon$ to $x = a + \varepsilon$, which yields:

$$EI\frac{\partial^3 \Delta w}{\partial x^3} - \frac{EI}{GA_s}K\frac{\partial \Delta w}{\partial x} + 0 = 0 - \frac{EI}{GA_s}\frac{\partial \Delta p}{\partial x}. \tag{5.20}$$

In Equation (5.20), the zero terms come from the assumptions of continuity of w and no point load in p at $x = a$. Additionally, in Equation (5.20) the terms Δw and Δp are defined by the following formula:

$$\Delta f \coloneqq \lim_{\varepsilon \to 0} \int_{a-\varepsilon}^{a+\varepsilon} \frac{\partial f(x)}{\partial x} dx = \lim_{\varepsilon \to 0} [f(a + \varepsilon) - f(a - \varepsilon)]. \tag{5.21}$$

Multiplying both sides of Equation (5.20) by $x - a$ and integrating by parts results in:

$$EI\frac{\partial^2 \Delta w}{\partial x^2} - \frac{EI}{GA_s}K\Delta w = -\frac{EI}{GA_s}\Delta p. \tag{5.22}$$

A further multiplication by $(x - a)^2$ and integrating by parts yields: $\frac{\partial \Delta w}{\partial x} = 0$, leading to the following four continuity conditions:

$$\Delta w = 0, \frac{\partial \Delta w}{\partial x} = 0, \Delta p = GA_s\frac{\partial^2 \Delta w}{\partial x^2}, \text{ and } \frac{\partial \Delta p}{\partial x} = GA_s\frac{\partial^3 \Delta w}{\partial x^3} \tag{5.23}$$

The four unknowns are determined through the imposition of these four continuity conditions.

To demonstrate the solution strategy developed above, consider the case of a beam weak in shear. Equation (5.14) in the semi-open interval $x \in [a, \infty)$, and the addition of Equations (5.18) and (5.19) in the interval $x \in [0, a]$, reduce to:

$$w(x) = Be^{-\alpha_2(x-a)} + De^{-\beta_2(x-a)} \text{ and } p(x) = Ecosh(\gamma_1 x) - K\Delta + \frac{Kx^2}{2R}, \tag{5.24}$$

respectively. Continuity condition of w and $\frac{\partial w}{\partial x}$ at $x = a$ are given by:

$$B + D = -\Delta + \frac{a^2}{2R} \text{ and } -\alpha_2 B - \beta_2 D = \frac{a}{R}. \tag{5.25}$$

Equations (5.25) can be used to determine B and D:

$$B = \frac{-1}{\alpha_2 - \beta_2}\left(\frac{a}{R} - \beta_2\Delta + \beta_2\frac{a^2}{2R}\right) \text{ and } D = \frac{1}{\alpha_2 - \beta_2}\left(\frac{a}{R} - \alpha_2\Delta + \alpha_2\frac{a^2}{2R}\right). \tag{5.26}$$

The jump in p at $x = a$ is $\Delta p = p^+ - p^-$, where $p^+ = 0$. Similarly, $\frac{\partial^2 \Delta w}{\partial x^2} = \left(\frac{\partial^2 w}{\partial x^2}\right)^+ - \left(\frac{\partial^2 w}{\partial x^2}\right)^-$. Thus, $\Delta p = GA_s \frac{\partial^2 \Delta w}{\partial x^2}$ becomes:

$$-\left(Ecosh(\gamma_1 a) - K\Delta + \frac{Ka^2}{2R}\right) = -GA_s\left(\alpha_2^2 B + \beta_2^2 D - \frac{1}{R}\right) \tag{5.27}$$

Carrying out the same process for $\frac{\partial \mathrm{p}}{\partial x}$ and $\frac{\partial^3 w}{\partial x^3}$ leads to:

$$-\left(Esinh(\gamma_1 a) + \frac{Ka}{R}\right) = -GA_s(\alpha_2^3 B + \beta_2^3 D). \tag{5.28}$$

Dividing Equation (5.27) and (5.28) by KR leads to

$$-\left(\bar{E}cosh(\gamma_1 a) - \frac{\Delta}{R} + \frac{a^2}{2R^2}\right) = -\frac{GA_s}{KR}\left(\alpha_2^2 B + \beta_2^2 D - \frac{1}{R}\right), \tag{5.29}$$

and

$$-\left(\bar{E}sinh(\gamma_1 a) + \frac{a}{R^2}\right) = -\frac{GA_s}{KR}(\alpha_2^3 B + \beta_2^3 D), \tag{5.30}$$

respectively. In Equations (5.29) and (5.30), $\bar{E} := \frac{E}{KR}$. From these two equations, the following two expressions are obtained for $\bar{E}$:

$$\begin{aligned} \bar{E}cosh(\gamma_1 a) &= \frac{\Delta}{R} - \frac{a^2}{2R^2} + \frac{GA_s}{KR}\left(\alpha_2^2 B + \beta_2^2 D - \frac{1}{R}\right) \\ \bar{E}sinh(\gamma_1 a) &= -\frac{a}{R^2}\frac{\Delta}{R} + \frac{GA_s}{KR}(\alpha_2^3 B + \beta_2^3 D) \end{aligned} \tag{5.31}$$

Eliminating $\bar{E}$ from these equations results in a single equation for a:

$$tanh(\gamma_1 a) = \frac{1}{\gamma_1}\frac{\frac{GA_S}{KR}(\alpha_2^3 B+\beta_2^3 D)-\frac{a}{R^2}}{\frac{GA_S}{KR}\left(\alpha_2^2 B+\beta_2^2 D-\frac{1}{R}\right)+\frac{\Delta}{R}-\frac{a^2}{2R^2}}. \tag{5.32}$$

Substituting the definition $\alpha^2 \coloneqq \frac{K}{GA_S}$ yields:

$$tanh(\gamma_1 a) = \frac{1}{\gamma_1}\frac{\alpha_2^3 B+\beta_2^3 D-\alpha^2\frac{a}{R}}{\alpha_2^2 B+\beta_2^2 D-\frac{1}{R}+\alpha^2\Delta-\alpha^2\frac{a^2}{2R^2}}. \tag{5.33}$$

Equation (5.33) expresses a in terms of Δ. However, because B and D are linear in Δ, it is more convenient to view it as expressing Δ in terms of a specified a. To this end, Equation (5.26) can be used to eliminate B and D from Equation (5.33), resulting in:

$$tanh(\gamma_1 a) = \frac{1}{\gamma_1}\frac{\alpha_2\beta_2(\alpha_2+\beta_2)\left(\Delta-\frac{a^2}{2R^2}\right)-(\alpha_2^2+\alpha_2\beta_2+\beta_2^2+\alpha^2)\frac{a}{R}}{(\alpha_2\beta_2+\alpha^2)\left(\Delta-\frac{a^2}{2R^2}\right)-(\alpha_2+\beta_2)\frac{a}{R}-\frac{1}{R}}. \tag{5.34}$$

Rewriting Equation (5.34) to express Δ in terms of a, after some rearrangements, gives:

$$\Delta = \frac{[(\alpha_2+\beta_2)\gamma_1 tanh(\gamma_1 a)-(\alpha_2^2+\alpha_2\beta_2+\beta_2^2+\alpha^2)]\frac{a}{R}}{\zeta}+\frac{a^2}{2R}-\frac{\gamma_1 tanh(\gamma_1 a)}{R\zeta}. \tag{5.35}$$

In Equation (5.35), $\zeta \coloneqq (\alpha_2\beta_2+\alpha^2)\gamma_1 tanh(\gamma_1 a)-\alpha_2\beta_2(\alpha_2+\beta_2)$. Substituting Equation (5.35) into the first of Equations (5.31) and taking advantage of Equation (5.26) yields:

$$\bar{E}cosh(\gamma_1 a) = \left(1+\frac{\alpha_2\beta_2}{\alpha^2}\right)\left(\frac{\Delta}{R}-\frac{a^2}{2R^2}\right)-\frac{\alpha_2+\beta_2}{\alpha^2 R}\frac{a}{R}-\frac{1}{\alpha^2 R^2} \tag{5.36}$$

Substituting Equation (5.36) into the pressure distribution expression, Equation (5.24b), yields:

$$p(x) = \left[\left(1+\frac{\alpha_2\beta_2}{\alpha^2}\right)\left(\frac{\Delta}{R}-\frac{a^2}{2R^2}\right)-\frac{\alpha_2+\beta_2}{\alpha^2 R}\frac{a}{R}-\frac{1}{\alpha^2 R^2}\right]\frac{cosh(\gamma_1 x)}{cosh(\gamma_1 a)}-\frac{\Delta}{R}+\frac{x^2}{2R^2}. \tag{5.37}$$

Equation (5.37) reveals that $p(a) \neq 0$.

Finally, the total applied force, F_{ext}, that is required to for a contact zone $x \in [-a, a]$, where a is a specified value, is obtained by the integral $F_{ext} = -2\int_0^a p dX$, which yields:

$$F_{ext} = 2\left[\frac{\alpha_2+\beta_2}{\alpha^2 R}\frac{a}{R}+\frac{1}{\alpha^2 R^2}-\left(1+\frac{\alpha_2\beta_2}{\alpha^2}\right)\left(\frac{\Delta}{R}-\frac{a^2}{2R^2}\right)\right]\frac{tanh(\gamma_1 a)1}{\gamma_1}+2\left(\frac{\Delta a}{R}-\frac{a^3}{6R^2}\right). \tag{5.38}$$

5.2 Elastic Shear Beam on Elastic Foundation; Roller Indentation

The solution derived in Section 5.1 for a beam weak in shear can be further simplified by setting $EI \to \infty$. In this case the governing equation, ignoring inertia, is given by:

$$\frac{\partial^4 w}{\partial x^4} = -\frac{1}{GA_s}\frac{\partial^2 p}{\partial x^2} \tag{5.39}$$

When the beam is resting on an elastic Winkler foundation, p is replaced by $p - Kv$, leading to:

$$\frac{\partial^4 w}{\partial x^4} - \frac{K}{GA_s}\frac{\partial^2 w}{\partial x^2} = -\frac{1}{GA_s}\frac{\partial^2 p}{\partial x^2} \tag{5.40}$$

Integrating Equation (5.40) twice leads to:

$$\frac{\partial^2 w}{\partial x^2} - \frac{K}{GA_s}w = -\frac{1}{GA_s}p \tag{5.41}$$

The constants of integration vanish from Equation (5.40) because the beam is assumed to be infinitely long.

When subjected to a rigid wheel of radius R, the beam-wheel contact zone is the interval $x \in [-a, a]$, where the symmetry about the origin holds only for the elastic case. Let c designate the point on the deformed surface, closest to a, where the transverse displacement $w = 0$. Denote the angle between the normal to the reference (*i.e.*, prior to deformation) surface at $x = 0$ and the line connecting points c and the center of the wheel as θ. The maximum transverse deflection, Δ, and the point c are related to θ and R through: $\Delta = R(1 - cos\theta)$ and $c = Rsin\theta$. Equipped with these geometrical relations, the transverse displacement in the contact zone can be expressed as:

$$w(x) = -\Delta\left(1 - \frac{x^2}{c^2}\right) \tag{5.42}$$

Furthermore, if $\Delta \ll R$ then c is given in terms of Δ as:

$$c^2 = 2R\Delta. \tag{5.43}$$

Substituting Equation (5.43) into Equation (5.42) yields:

$$w(x) = -\Delta\left(1 - \frac{x^2}{2R\Delta}\right), \frac{\partial w(x)}{\partial x} = \frac{\mathrm{x}}{R}, \frac{\partial^2 w(x)}{\partial x^2} = \frac{1}{R}, \text{ and } \frac{\partial^3 w(x)}{\partial x^3} = 0. \tag{5.44}$$

Remark: Identifying the curvature, $\frac{\partial^2 w}{\partial x^2}$, with $\frac{1}{R}$ is valid *only* for the case where $\Delta \ll R$.♦

Beyond the contact area (*i.e.*, $x \in [a, \infty)$) $p = 0$, and the Equation (5.41) reduces to:

$$\frac{\partial^2 w}{\partial x^2} - \alpha^2 w = 0 \tag{5.45}$$

In Equation (5.45) $\alpha^2 \coloneqq \frac{K}{GA_s}$. The solution to Equation (5.45) can be written as:

$$w(x) = Ae^{-\alpha(x-a)}. \tag{5.46}$$

The constant term in the exponential, αa, in Equation (5.46) is introduced in order to simplify the subsequent development. It amounts to a redefinition of the constant A. Equation (5.46)

contains two unknowns: A and a, which, in the absence of a point load at $x = a$, can be determined by imposing continuity of w and $\frac{\partial w}{\partial x}$ at $x = a$ to obtain:

$$w(a) = -\Delta\left(1 - \frac{a^2}{c^2}\right) = A \text{ and } \frac{\partial w(a)}{\partial x} = \frac{2a\Delta}{c^2} = -\alpha A. \tag{5.47}$$

Eliminating A From Equations (5.47) gives:

$$\Delta\left(1 - \frac{a^2}{c^2}\right) = \frac{2a\Delta}{\alpha c^2}. \tag{5.48}$$

Equation (5.48) leads to the following equation for $\frac{a}{c}$:

$$\frac{a^2}{c^2} + \frac{2a}{c}\frac{1}{\alpha c} - 1 = 0. \tag{5.49}$$

The solution to Equation (5.49) is given by (only the positive root is considered because $a \geq 0$):

$$\frac{a}{c} = -\frac{1}{\alpha c} + \sqrt{1 + \frac{1}{a^2 c^2}}. \tag{5.50}$$

Rewriting Equation (5.50) in terms of Δ and R gives:

$$\frac{a}{R} = -\frac{1}{\alpha R} + \frac{1}{\alpha R}\sqrt{1 + 2a^2 R^2 \frac{\Delta}{R}}. \tag{5.51}$$

If $\Delta \ll R$ Equation (5.51) can be approximated by:

$$\frac{a}{R} = \alpha R \frac{\Delta}{R} - \frac{1}{2} a^3 R^3 \left(\frac{\Delta}{R}\right)^2. \tag{5.52}$$

In the contact zone the pressure can be determined by substituting Equation (5.42) into Equation (5.40), which results in:

$$p(x) = -\frac{GA_S}{R} - K\Delta\left(1 - \frac{x^2}{c^2}\right) \approx -\frac{GA_S}{R}\left(1 + \alpha^2 \Delta\mathrm{R} - \frac{\alpha^2 x^2}{2}\right). \tag{5.53}$$

The approximation in Equation (5.53) is valid only when if $\Delta \ll R$, in which case c^2 is approximated by Equation (5.43). Equation (5.53) reveals that $p(a) \neq 0$. It is given by:

$$p(a) \approx -\frac{GA_S}{R}(1 + 2\alpha^2 \Delta\mathrm{R}). \tag{5.54}$$

An examination of Equations (5.52) and (5.54) reveals that as $\Delta \to 0$, the contact zone a $\to 0$ but p does not. This unexpected result is due to the fact that $\frac{\partial w}{\partial x} \approx \frac{1}{R}$ and so does not vanish as a $\to 0$. The applied load is given by:

$$F_{ext} = -2\int_0^a p(x)dx \approx 2a\frac{GA_S}{R}\left(1 + \alpha^2 \Delta\mathrm{R} - \frac{\alpha^2 a^2}{6}\right). \tag{5.55}$$

Substituting Equation (5.52) into Equation (5.55) yields:

$$F_{ext} = \frac{4GA_s}{3\alpha R}\left[\sqrt{1+\alpha^2\Delta\mathrm{R}} - 1\right]\left[1 + \alpha^2\Delta\mathrm{R} + 2\sqrt{1+\alpha^2\Delta\mathrm{R}}\right]. \tag{5.56}$$

It is evident from Equation (5.55) and Equation (5.56) that although $p \nrightarrow 0$ as a $\rightarrow 0$, $F_{ext} \rightarrow 0$.

5.3 Elastic Shear Bean on a Kelvin-Voigt Foundation; Roller Indentation

The elastic foundation considered in Section 5.2 is now replaced with a viscoelastic Kelvin-Voigt foundation so that the (foundation's) reaction Kw is now replaced by $K\left(w + \tau\frac{\partial w}{\partial t}\right)$, where τ is the characteristic time of the foundation material. In this case, the governing equation replacing Equation (5.41) is given by:

$$-GA_s\frac{\partial^2 w}{\partial x^2} + K\left(w - \tau v\frac{\partial w}{\partial x}\right) = p(x) \tag{5.57}$$

Note that Equation (5.57) is set relative to the moving coordinate system (see Section 2.2), and that inertia is ignored. Further note that if either $v \rightarrow 0$ or $\tau \rightarrow 0$, the problem is reduced to the elastic case considered in Section 5.2.

For the case considered in this section, symmetry of the solution about the origin can no longer be assumed. The contact region is now taken as the interval $x \in [-b, a]$. The expression for the transverse displacement in the contact region, however, remains as in Section 5.2 and is given by Equation (5.44).

Outside the contact zone, the pressure is zero, and Equation (5.57) reduces to:

$$-GA_s\frac{\partial^2 w}{\partial x^2} + K\left(w + \tau v\frac{\partial w}{\partial x}\right) = 0. \tag{5.58}$$

Define $\alpha^2 \coloneqq \frac{K}{GA_s}$. With this definition Equation (5.58) can be rewritten as:

$$\frac{\partial^2 w}{\partial x^2} + \alpha^2 v\tau\frac{\partial w}{\partial x} - \alpha^2 w = 0 \tag{5.59}$$

The solution to Equation (5.59) is of the form $w = e^{\lambda x}$, which leads to the following characteristic equation:

$$\lambda^2 + \alpha^2 v\tau\lambda - \alpha^2 = 0. \tag{5.60}$$

The solutions to Equation (5.60) is given by:

$$\begin{aligned}\lambda_1 &= \tfrac{1}{2}\left(\alpha^2 v\tau + \sqrt{\alpha^4 v^2\tau^2 + 4\alpha^2}\right) = \tfrac{\alpha^2 v\tau}{2}\left(1 + \sqrt{1 + \tfrac{4}{\alpha^2 v^2\tau^2}}\right)\\ \lambda_2 &= \tfrac{1}{2}\left(-\alpha^2 v\tau - \sqrt{\alpha^4 v^2\tau^2 + 4\alpha^2}\right) = \tfrac{\alpha^2 v\tau}{2}\left(-1 + \sqrt{1 + \tfrac{4}{\alpha^2 v^2\tau^2}}\right)\end{aligned} \tag{5.61}$$

In Equation (5.61), $\lambda_1 < 0$, $\lambda_2 > 0$, and $|\lambda_1| > \lambda_2$. Thus, the solution for the w outside the contact zone is given by:

$$\begin{aligned} w(x) &= Ae^{\lambda_1(x-a)} \quad a \le x \le \infty \\ w(x) &= Be^{\lambda_2(x+b)} \quad \infty \le x \le -b \end{aligned} \tag{5.62}$$

In Equations (5.62) the addition of $-a$ and b in the exponential amounts to reparameterizing of the constants A and B. They are introduced in order to simplify imposing continuity conditions in the subsequent development.

Within the contact zone, $w(x)$ is given by Equation (5.44). Assuming that w and $\frac{\partial w}{\partial x}$ are continuous at $x = a$ and $x = -b$ (*i.e.*, there are no point loads at the ends of the contact zone), the following expressions for w and $\frac{\partial w}{\partial x}$ at points a and $-b$ are obtained:

$$\begin{aligned} w(a) &= -\Delta + \frac{a^2}{2R} = A \quad and \quad \frac{\partial w(a)}{\partial x} = \frac{a}{R} = \lambda_1 A \\ w(-b) &= -\Delta + \frac{b^2}{2R} = B \quad and \quad \frac{\partial w(-b)}{\partial x} = -\frac{b}{R} = \lambda_2 B \end{aligned} \tag{5.63}$$

Equations (5.63) lead, after some manipulations, to the solution:

$$\begin{aligned} \frac{a}{R} &= \frac{1}{\lambda_1 R}\left(-1 + \sqrt{1 + 2\lambda_1^2 R^2 \frac{\Delta}{R}}\right) \\ \frac{b}{R} &= \frac{1}{\lambda_2 R}\left(-1 + \sqrt{1 + 2\lambda_2^2 R^2 \frac{\Delta}{R}}\right) \end{aligned} \tag{5.64}$$

Note that as $\Delta \to 0$, a $\to 0$ and b $\to 0$. Furthermore, $b \le a$ when $\Delta \neq 0$. Finally, using Equations (5.63), values of the constants A and B are given by:

$$\begin{aligned} \frac{A}{R} &= \frac{1}{\lambda_1^2 R^2}\left(1 - \sqrt{1 + 2\lambda_1^2 R^2 \frac{\Delta}{R}}\right) \approx -\frac{\Delta}{R} + \frac{1}{2}\lambda_1^2 R^2 \frac{\Delta^2}{R^2} \\ \frac{B}{R} &= \frac{1}{\lambda_2^2 R^2}\left(1 - \sqrt{1 + 2\lambda_2^2 R^2 \frac{\Delta}{R}}\right) \approx -\frac{\Delta}{R} + \frac{1}{2}\lambda_2^2 R^2 \frac{\Delta^2}{R^2} \end{aligned} \tag{5.65}$$

Equations (5.65) demonstrate that as the indentation proceeds, A and B start with the same value. As the indentation, Δ, increases, the value of $|B|$ increases more rapidly than that of $|A|$.

The pressure within the contact zone is given by:

$$p(x) = -GA_s \frac{\partial^2 w}{\partial x^2} + Kw - K\nu\tau \frac{\partial w}{\partial x}. \tag{5.66}$$

Substituting the displacement field within the contact zone, given by Equations (5.44), into Equation (5.66) yields:

$$p(x) = -\frac{GA_s}{R} - K\Delta + K\frac{x^2}{2R} - Kv\tau\frac{x}{R}. \tag{5.67}$$

The total applied force is given by:

$$F_{ext} = -\left(\int_{-b}^{a} p dx = KR\left(\frac{1}{\alpha^2R^2} + \frac{\Delta}{R}\right)(a+b) - \frac{a^3+b^3}{6R^2} + \frac{v\tau}{2}\frac{a^2-b^2}{R}\right). \tag{5.68}$$

The asymmetry of the pressure distribution, due to viscosity, gives rise to a horizontal force, which is denoted here by H. The simplest way to calculate H is through work balance consideration. In particular, the rate of work done by the horizontal force is Hv, and the rate of work done by the vertical work is given by: $\int_{-b}^{a} -p(x)\, v\frac{\partial w}{\partial x} dx$. Equating the two rates of work expressions, and in view of Equation (5.44), leads to the following expression for the horizontal force:

$$H = -\int_{-b}^{a} p(x)\frac{\partial w}{\partial x} dx = -\int_{-b}^{a} p(x)\frac{x}{R} dx. \tag{5.69}$$

Substituting Equation (5.67) into Equation (5.69) leads to the following expression for the horizontal force:

$$H = \frac{K}{2}\left[\left(\frac{1}{\alpha^2R^2} + \frac{\Delta}{R}\right)(a^2-b^2) - \frac{1}{4R^2}(a^4-b^4) + \frac{2v\tau}{3R^2}(a^3+b^3)\right]. \tag{5.70}$$

This result depends separately on Δ and $v\tau$. However, Equation (5.70) reveals that as $v\tau \to 0$, $a \to b$ and $H \to 0$.

Finally, the result for the vertical and horizontal forces can be used to define a rolling friction resistance factor, μ, that is obtained from the relation: $H = \mu F_{ext}$. Substituting Equation (5.68) and (5.70) yields the rolling friction resistance factor:

$$\mu = \frac{a-b}{2R}\frac{\left[\frac{1}{\alpha^2R^2} + \frac{\Delta}{R} - \frac{1}{4R^2}(a^2+b^2) + \frac{2v\tau(a^3+b^3)}{3R^2(a^2-b^2)}\right]}{\left[\frac{1}{\alpha^2R^2} + \frac{\Delta}{R} - \frac{1}{6R^2}(a^2-ab+b^2) + \frac{v\tau}{2R^2}(a-b)\right]}. \tag{5.71}$$

5.4 Elastic Shear Beam on Maxwell Foundation; Roller Indentation

In a one-dimensional setup, the Maxwell model relation between the stress, σ, and strain, ε, is given by:

$$E\frac{\partial \varepsilon}{\partial t} = \frac{\partial \sigma}{\partial t} + \frac{\sigma}{\tau}. \tag{5.72}$$

In Equation (5.72), τ is the characteristic time of the Maxwell element, and E is the instantaneous elastic stiffness of the Maxwell element. When transformed to a moving coordinate system, traveling at a constant velocity, v, Equation (5.72) takes the form:

$$E\frac{\partial \varepsilon}{\partial x} = \frac{\partial \sigma}{\partial x} - \frac{\sigma}{v\tau} \tag{5.73}$$

When this model is applied to represent the foundation's response, then Equation (5.41), representing an elastic beam weak in shear resting on an elastic foundation, becomes:

$$-v\tau GA_s\frac{\partial^3 w}{\partial x^3}+GA_s\frac{\partial^2 w}{\partial x^2}+v\tau K\frac{\partial w}{\partial x}=v\tau\frac{\partial p}{\partial x}-p \tag{5.74}$$

As in Section 5.3, the contact zone is defined as the interval $x\in[-b,a]$, where a and b are unknown to be determined by the solution. Outside the contact zone $p=0$, so that equation (5.74) is reduced to:

$$-v\tau GA_s\frac{\partial^3 w}{\partial x^3}+GA_s\frac{\partial^2 w}{\partial x^2}+v\tau K\frac{\partial w}{\partial x}=0. \tag{5.75}$$

As in previous sections, let $\alpha^2:=\frac{K}{GA_s}$, and define $s:=\frac{1}{v\tau}$. Equation (5.75) can be rewritten as:

$$\frac{\partial^3 w}{\partial x^3}-s\frac{\partial^2 w}{\partial x^2}-\alpha^2\frac{\partial w}{\partial x}=0. \tag{5.76}$$

The solution to Equation (5.76) is of the form $w=e^{\lambda x}$, which gives rise to the following characteristic equation: $\lambda^3-s\lambda^2-\alpha^2\lambda=0$. This equation has the following three roots:

$$\lambda_1=0,\ \lambda_2=\frac{s}{2}+\sqrt{\frac{s^2}{4}+\alpha^2}=:\alpha_1,\text{ and }\lambda_3=\frac{s}{2}-\sqrt{\frac{s^2}{4}+\alpha^2}=:-\alpha_2 \tag{5.77}$$

Thus, in the interval $x\in(-\infty,b]$, the solution is given by:

$$w(x)=A+Be^{\alpha_1(x+b)}, \tag{5.78}$$

and in the interval $x\in[a,\infty)$ the solution is given by:

$$w(x)=Ce^{-\alpha_2(x-a)}. \tag{5.79}$$

The unknowns a and b appearing in the exponentials in Equations (5.78) and (5.79) amount to reparameterizing of the constants B and C. They are included to simplify imposing continuity conditions in the pursuant development.

In the contact zone, $x\in[-b,a]$, Equation (5.74) can be rewritten as:

$$GA_s\left(-\frac{\partial^3 w}{\partial x^3}+s\frac{\partial^2 w}{\partial x^2}+\alpha^2\frac{\partial w}{\partial x}\right)=\frac{\partial p}{\partial x}-sp. \tag{5.80}$$

The derivatives of the transverse displacement, w, are given by Equation (5.44). The homogenous complimentary solution is $p(x)=De^{sx}$, and the particular solution takes the form: $p=-GA_s\frac{1}{R}-\frac{1}{s}K\frac{x}{R}-\frac{1}{s^2}K\frac{1}{R}$. Thus, the equation for $p(x)$ in the contact area is given by:

$$p(x)=De^{s(x-a)}-\frac{GA_s}{R}\left(1+\frac{\alpha^2}{s^2}+\frac{\alpha^2 x}{s}\right). \tag{5.81}$$

For the interval $x \in [a, \infty)$ w is given by Equation (5.79), with $w(a) = -\Delta + \frac{a^2}{2R}$ and $\frac{\partial w(a)}{\partial x} = \frac{a}{R}$. Thus, $C = -\Delta + \frac{a^2}{2R}$, and a is given by:

$$a = -\frac{1}{\alpha_2} + \sqrt{\frac{1}{\alpha_2^2} + 2R\Delta} \tag{5.82}$$

Next, behind the moving wheel, $x \in (-\infty, b)$, the transverse displacement is given by Equation (5.78), so that at $x = -b$

$$w(-b) = -\Delta + \frac{b^2}{2R} = A + B \text{ and } \frac{\partial w(-b)}{\partial x} = -\frac{b}{R} = \alpha_1 B. \tag{5.83}$$

Using Equations (5.83) A and B can be expressed in terms of Δ and b as:

$$B = -\frac{b}{\alpha_1 R} \text{ and } A = -\Delta + \frac{b^2}{2R}\left(1 + \frac{2}{\alpha_1 b}\right). \tag{5.84}$$

To determine b, recall that the pressure within the contact zone is given by Equation (5.81), and consider the jump conditions at the ends of the contact zone, under the assumption that w and $\frac{\partial w}{\partial x}$ are both continuous at both ends. (These assumptions preclude point loads at the ends of the contact zone.) The equation governing the motion in the contact zone is given by Equation (5.74). Integrating Equation (5.74) across the jump at $x = a$ (in a manner analogous to the integration of Equation (5.21)) and taking the limit as $\varepsilon \to 0$ leads to:

$$-v\tau G A_s \frac{\partial^2 w}{\partial x^2} + G A_s \frac{\partial w}{\partial x} + v\tau K \Delta w = \Delta p - 0. \tag{5.85}$$

The last zero in Equation (5.85) is because a point load at $x = a$ is not allowed. It follows from Equation (5.85) and the continuity assumptions that:

$$\Delta p = -G A_s \frac{\partial^2 w}{\partial x^2}. \tag{5.86}$$

Recalling that on the contact side of point a, $\frac{\partial^2 (a^-)}{\partial x^2} = \frac{1}{R}$, while just outside the contact zone $\frac{\partial^2 (a^+)}{\partial x^2} = \alpha_2^2 C$, the following result is obtained for the pressure just inside the contact zone:

$$p(a^-) = -\frac{GA_s}{R}(1 + \alpha_2 a). \tag{5.87}$$

Arriving at Equation (5.87) took advantage of the known result: $p(a^+) = 0$. Following a similar procedure at $x = -b$ results in:

$$p(-b^+) = -\frac{GA_s}{R}(1 + \alpha_1 b) \tag{5.88}$$

Substituting Equations (5.86) into Equation (5.80) gives:

$$D = \frac{GA_s}{R}\left[\frac{\alpha^2}{s^2} + \frac{\alpha^2}{s^2}sa - \frac{\alpha^2}{s}sa\right] \tag{5.89}$$

The boundary condition at $x = -b$ provides the defining equation for the unknown b, given by:

$$\left(\frac{\alpha^2}{s^2} - \frac{\alpha^2}{s^2}sb - \frac{\alpha_1}{s}sb\right)e^{sb} = \left(\frac{\alpha^2}{s^2} + \frac{\alpha^2}{s^2}sa - \frac{\alpha_2}{s}sa\right)e^{-sa} \tag{5.90}$$

Note that a $\to 0$ as $\Delta \to 0$, which leads to b $= 0$. Once b is determined, the constants A, B, and C can be obtained, determining the deformed shape of the beam.

Remark: The value of A shows the permanent displacement after the passage of the wheel. ♦

The above derivation determines the displacement field for a given prescribed indentation. To determine the applied force, F_{ext}, the expression for the pressure, Equation (5.80), is integrated over the contact zone to obtain:

$$\frac{sRF_{ext}}{GA_S} = \left(\frac{\alpha^2}{s^2} + \frac{\alpha^2}{s^2}sa - \frac{\alpha_2}{s}sa\right)\left(e^{-s(a+b)} - 1\right) - \left(1 + \frac{\alpha^2}{s^2}\right)s(a+b) - \frac{\alpha^2}{s^2}(a^2 - b^2) \tag{5.91}$$

Finally, the horizontal force, H, caused by the non-symmetry of the pressure distribution can be calculated by equating the rate of work it does with the rate of work done by the applied vertical force. Accordingly, H can be obtained by substituting into Equation (5.68) the expression obtained for the vertical force, Equation (5.91), to obtain:

$$\frac{sRH}{GA_S} = -\zeta\left(sa - 1 + \frac{\alpha^2}{s^2}sae^{-s(a+b)}\right) - \left(\left(1 + \frac{\alpha^2}{s^2}\right)\frac{s^2}{2}(a^2 - b^2) + \frac{\alpha^2}{s^2}\frac{(a^3 - b^3)}{3}\right) \tag{5.92}$$

In Equation (5.92), $\zeta = \frac{\alpha^2}{s^2} + \frac{\alpha^2}{s^2}sa - \frac{\alpha_2}{s}sa$. As in Section 5.3, H depends separately on the indentation, Δ, and on the characteristic length $v\tau$. Note that when $v\tau \to 0$, then $a \to b$, and consequently $H \to 0$. Finally, the result for the vertical and horizontal forces can be used to define a rolling friction resistance factor, μ, that is obtained from the relation: $H = \mu F_{ext}$.

5.5 Maxwell Shear Beam on Maxwell Foundation; Roller Indentation

The response for a Maxwell element is described by Equation (5.72). Applying this law to the case of a beam weak in shear where the beam and foundation are each represented by a single Maxwell element that share the same characteristic period is given, in the moving coordinate system, by:

$$v\tau\left(GA_s\frac{\partial^3 w}{\partial x^3} - K\frac{\partial w}{\partial x}\right) = p - v\tau\frac{\partial p}{\partial x}. \tag{5.93}$$

As in previous sections, let $\alpha^2 \coloneqq \frac{K}{GA_S}$, and define $s \coloneqq \frac{1}{v\tau}$. Equation (5.93) can be rewritten as:

$$\frac{\partial^3 w}{\partial x^3} - \alpha^2\frac{\partial w}{\partial x} = \frac{1}{GA_S}\left(sp - \frac{\partial p}{\partial x}\right) \tag{5.94}$$

Outside the contact zone, a solution of the form $w = e^{\lambda x}$ leads to the following characteristic polynomial:

$$\lambda(\lambda^2 - \alpha^2) = 0. \tag{5.95}$$

The roots are: $\lambda = 0$, and $\lambda = \pm\alpha$. Thus, behind the wheel, $x \in (-\infty, -b]$, the transverse displacement is given by:

$$w(x) = A + Be^{\alpha(x+b)}. \tag{5.96}$$

In front of the wheel, $x \in [a, \infty)$, the solution is given by:

$$w(x) = Ce^{-\alpha(x-a)}. \tag{5.97}$$

In the contact zone, the pressure is determined by using Equation (5.94). (Recall that the deformation there is prescribed; Δ is taken as given.) The complementary homogeneous solution is given by:

$$p_h(x) = GA_sDe^{s(x-a)}. \tag{5.98}$$

In Equation (5.98), D is a constant to be determined along with A, B, and C. Since $\frac{\partial^3 w}{\partial x^3} = 0$ in the contact zone, Equation (5.94) becomes:

$$sp - \frac{\partial p}{\partial x} = -GA_s\alpha^2\frac{x}{R} \tag{5.99}$$

The particular solution to equation (5.99) is given by:

$$p_p(x) = -\frac{GA_s}{s}\frac{\alpha^2}{R}\left(x + \frac{1}{s}\right). \tag{5.100}$$

Thus, the pressure distribution in the contact area is give by:

$$p(x) = p_h(x) + p_p(x) = GA_s\left(De^{s(x-a)} - \frac{\alpha^2}{s}\frac{x}{R} - \frac{\alpha^2}{s^2}\frac{1}{R}\right). \tag{5.101}$$

Assuming continuity of w at $x = a$, and in view of Equation (5.97) and the prescribed displacement on the inner side of the contact zone (see Equation (5.42)), a and C are given by:

$$C = -\frac{a}{\alpha R} \text{ and } a = -\frac{1}{\alpha} + \sqrt{\frac{1}{\alpha^2} + 2R\Delta}. \tag{5.102}$$

Behind the wheel, $x \in (-\infty, -b]$, the transverse displacement is given by Equation (5.96), which when combined with the known transverse displacement and its first derivative at $x = -b$ leads to:

$$A = -\Delta + \frac{b^2}{2R}\left(1 + \frac{2}{\alpha b}\right) \text{ and } B = -\frac{b}{\alpha R}. \tag{5.103}$$

Note that in Equation (5.103), b is unknown. It is determined by equating the expression for the pressure, given by Equation (5.101), with the pressure jump at $x = a$. The expression for the pressure jump is obtained by integrating Equation (5.99), which, under the assumption of no point load at $x = a$, yields:

$$-\Delta p = GA_s\left(\frac{\partial^2 \Delta \mathrm{w}}{\partial \mathrm{x}^2} - \alpha^2 \Delta \mathrm{w}\right). \tag{5.104}$$

Equating the pressure jump, Equation (5.104), with the pressure, Equation (5.101), at $x = a^-$ (*i.e.,* just inside the contact zone), with the help of Equations (5.97) and (5.42) and their derivatives, leads to:

$$D = \frac{1}{R}\left(\frac{\alpha^2}{s}a + \frac{\alpha^2}{s^2} - \alpha a - 1\right). \tag{5.105}$$

Substituting Equation (5.105) into Equation (5.101) yields the following expression for the pressure distribution:

$$p(x) = \frac{GA_s}{R}\left[\left(1 + \alpha a - \frac{\alpha^2 a}{s} - \frac{\alpha^2}{s^2}\right)e^{s(x-a)} - \frac{\alpha^2}{s}x - \frac{\alpha^2}{s^2}\right]. \tag{5.106}$$

Evaluating Equation (5.106) at $x = -b$, and equating it with the pressure jump at that location, leads to the following equation for b:

$$\left(1 + \alpha a - \frac{\alpha^2 a}{s} - \frac{\alpha^2}{s^2}\right)e^{-s(a+b)} + \left(\frac{\alpha^2}{s} + \alpha\right)b = \frac{\alpha^2}{s^2} - 1. \tag{5.107}$$

Once all the parameters are determined, the pressure can be integrated over the contact zone to obtain the total vertical force. Finally, the horizontal force and friction coefficient can be deduced from the energy balance.

5.6 Maxwell Beam on Maxwell Foundation; Specified Load

The previous five subsections addressed the response of Timoshenko beams on Winkler foundations for different material models and when subjected to a rolling rigid wheel moving at a constant velocity. This section considers the response when the beam-foundation system is loaded by a uniform load per unit length, p_0, applied to the center segment of the beam, $x \in [-a, a]$. Additionally, a Maxwell element material response is considered for the bending, shear, and foundation responses.

The governing equation for an elastic beam-foundation, relative to a moving coordinate system, is given by Equation (5.3), which can be recast into an operator form as:

$$\left(EI\frac{\partial^4}{\partial x^4} - \frac{EI}{GA_s}K\frac{\partial^2}{\partial x^2} + K\right)w = \left(1 - \frac{EI}{GA_s}\frac{\partial^2}{\partial x^2}\right)p. \tag{5.108}$$

Similarly, the stress-strain relation for a one-dimensional Maxwell element, relative to a moving coordinate system, which is given by Equation (5.73), can be recast into the following operator form:

$$\left(E\frac{\partial}{\partial x}\right)\varepsilon = \left(\frac{\partial}{\partial x} - \frac{1}{\tau v}\right)\sigma. \tag{5.109}$$

Combining the equations leads to the governing equation for a viscoelastic beam-foundation system where all three responses (*i.e.*, bending, shear, and foundation) are represented by Maxwell elements with the same characteristic period (*i.e.*, $\tau_b = \tau_s = \tau_f = \tau$):

$$EI\frac{\partial^5 w}{\partial x^5} - \frac{EI}{GA_s}K\frac{\partial^3 w}{\partial x^3} + K\frac{\partial w}{\partial x} = \frac{\partial p}{\partial x} - \frac{p}{\tau v} - \frac{EI}{GA_s}\left(\frac{\partial^3 p}{\partial x^3} - \frac{1}{\tau v}\frac{\partial^2 p}{\partial x^2}\right). \tag{5.110}$$

Equation (5.110) can be split into two parts where $w = w^e + w^v$. $w^e(x)$ is the elastic solution obtained by solving the following equation:

$$EI\frac{\partial^4 w^e}{\partial x^5} - \frac{EI}{GA_s}K\frac{\partial^2 w^e}{\partial x^2} + Kw^e = p - \frac{EI}{GA_s}\frac{\partial^2 p}{\partial x^2}. \tag{5.111}$$

Note that to arrive at Equation (5.111) required integrating Equation (5.110). $w^v(x)$ is the viscous solution obtained by solving the following equation:

$$EI\frac{\partial^5 w^v}{\partial x^5} - \frac{EI}{GA_s}K\frac{\partial^3 w^v}{\partial x^3} + K\frac{\partial w^v}{\partial x} = -\frac{1}{\tau v}\left(p - \frac{EI}{GA_s}\frac{\partial^2 p}{\partial x^2}\right). \tag{5.112}$$

Define $\alpha^2 \coloneqq \frac{K}{GA_s}$ and $\beta^4 \coloneqq \frac{K}{EI}$. Substituting these definitions into Equations (5.111) and (5.112) yields:

$$\frac{\partial^4 w^e}{\partial x^5} - \alpha^2\frac{\partial^2 w^e}{\partial x^2} + \beta^4 w^e = \frac{1}{EI}\left(p - \frac{\alpha^2}{\beta^4}\frac{\partial^2 p}{\partial x^2}\right) \tag{5.113}$$

and

$$\frac{\partial^5 w^v}{\partial x^5} - \alpha^2\frac{\partial^3 w^v}{\partial x^3} + \beta^4\frac{\partial w^v}{\partial x} = -\frac{1}{\tau v EI}\left(p - \frac{\alpha^2}{\beta^4}\frac{\partial^2 p}{\partial x^2}\right), \tag{5.114}$$

respectively.

5.6.1 Solution for w^e

For the loading assumption considered here, the particular solution to Equation (5.113) is $\frac{p_0}{EI\beta^4} = \frac{p_0}{K}$. The complimentary homogenous solution is in the form $w^e = e^{\lambda x}$, which results in the following characteristic polynomial:

$$\lambda^4 - \alpha^2\lambda^2 + \beta^4 = 0. \tag{5.115}$$

The four roots of Equation (5.115) are:

$$\lambda_1 = +\frac{\alpha}{2}\sqrt{1+\sqrt{1-\frac{4\beta^4}{\alpha^4}}} =: +\alpha_2 \quad \lambda_2 = -\frac{\alpha}{2}\sqrt{1+\sqrt{1-\frac{4\beta^4}{\alpha^4}}} =: -\alpha_2$$
$$\lambda_3 = +\frac{\alpha}{2}\sqrt{1-\sqrt{1-\frac{4\beta^4}{\alpha^4}}} =: +\beta_2 \quad \lambda_4 = -\frac{\alpha}{2}\sqrt{1-\sqrt{1-\frac{4\beta^4}{\alpha^4}}} =: -\beta_2 \tag{5.116}$$

The solution behind, under, and in front of the load, when $\frac{4\beta^4}{\alpha^4} < 1$ (*i.e.*, for a beam weak in shear), is given by:

$$\begin{aligned} w^e(x) &= B_1 e^{\alpha_2(x+a)} + C_1 e^{\beta_2(x+a)} && x \in (-\infty, -a] \\ w^e(x) &= E_1 e^{\alpha_2(x+a)} + F_1 e^{\beta_2(x+a)} + G_1 e^{-\alpha_2(x-a)} + H_1 e^{-\beta_2(x-a)} + \frac{p_0}{K} && x \in [-a, a] \\ w^e(x) &= I_1 e^{-\alpha_2(x-a)} + J_1 e^{-\beta_2(x-a)} && x \in [x, \infty] \end{aligned} \tag{5.117}$$

The elastic solution is symmetric about the origin, $x = 0$. Taking advantage of this observation, and using the symmetry of the hyperbolic cosine, the solution can be recast as:

$$\begin{aligned} w^e(x) &= 2G_1 Cosh(\propto_2 x) + 2H_1 Cosh(\beta_2 x) + \frac{p_0}{K} && x \in [-a, a] \\ w^e(x) &= I_1 e^{-\alpha_2(x-a)} + J_1 e^{-\beta_2(x-a)} && x \in [a, \infty] \end{aligned} \tag{5.118}$$

The four unknowns can be determined by enforcing continuity of w^e and its first three derivatives at $x = a$. These continuity conditions are:

$$\begin{aligned} w^e(a) &= 2G_1 Cosh(\propto_2 a) + 2H_1 Cosh(\beta_2 a) + \frac{p_0}{K} = I_1 + J_1 \\ \frac{\partial w^e(a)}{\partial x} &= 2 \propto_2 G_1 Sinh(\propto_2 a) + 2\beta_2 H_1 Sinh(\propto_2 a) = -\propto_2 I_1 - \beta_2 J_1 \\ \frac{\partial^2 w^e(a)}{\partial x^2} &= 2\alpha_2^2 G_1 Cosh(\propto_2 a) + 2\beta_2^2 H_1 Cosh(\propto_2 a) = \alpha_2^2 I_1 + \beta_2^2 J_1 \\ \frac{\partial^3 w^e(a)}{\partial x^3} &= 2\alpha_2^3 G_1 Sinh(\propto_2 a) + 2\beta_2^3 H_1 Sinh(\propto_2 a) = -\alpha_2^3 I_1 - \beta_2^3 J_1 \end{aligned} \tag{5.119}$$

This system of four equations can be readily solved for the four constants required in order to determine w^e.

5.6.2 Solution for w^v

The complimentary homogenous solution is given by: $w^v = e^{\lambda x}$, which leads to the following characteristic equation:

$$\lambda(\lambda^4 - \alpha^2\lambda + \beta^4) = 0. \tag{5.120}$$

The roots for this equation are $\lambda = 0$, and

$$\lambda_1 = +\frac{\alpha}{\sqrt{2}}\sqrt{1+\sqrt{1-\frac{4\beta^4}{\alpha^4}}} =: +\alpha_2 \quad \lambda_2 = -\frac{\alpha}{\sqrt{2}}\sqrt{1+\sqrt{1-\frac{4\beta^4}{\alpha^4}}} =: -\alpha_2$$
$$\lambda_3 = +\frac{\alpha}{\sqrt{2}}\sqrt{1-\sqrt{1-\frac{4\beta^4}{\alpha^4}}} =: +\beta_2 \quad \lambda_4 = -\frac{\alpha}{\sqrt{2}}\sqrt{1-\sqrt{1-\frac{4\beta^4}{\alpha^4}}} =: -\beta_2 \tag{5.121}$$

The solution for w^v, when the beam-foundation system is subjected to a constant load applied to the interval $x \in [-a, a]$, is given by:

$$\begin{aligned} w^v &= A + Be^{\alpha_2(x+a)} + Ce^{\beta_2(x+a)} && x \in (-\infty, -a] \\ w^v &= D + Ee^{\alpha_2(x+a)} + Fe^{\beta_2(x+a)} + Ge^{-\alpha_2(x-a)} + He^{-\beta_2(x-a)} + \bar{p}x && x \in [-a, a] \\ w^v &= Ie^{-\alpha_2(x-a)} + Je^{-\beta_2(x-a)} && x \in [a, \infty] \end{aligned} \tag{5.122}$$

$\bar{p}$ appearing in Equation (5.122) is defined as $\bar{p} := \frac{p_0}{v\tau K}$. Ten unknowns appear in Equations (5.122) that must be determined to compete the solution. They can be obtained by imposing continuity of $w^v$and its first four derivatives at $x = -a$ and $x = a$. (Recall that the governing equation, Equation (5.114), is fifth order.) The ten equations, cast in matrix form, are given by:

$$\begin{bmatrix} 1 & 1 & 1 & -1 & -1 & -1 & -e^{2\alpha_2 a} & -e^{2\beta_2 a} & 0 & 0 \\ 0 & 0 & 0 & 1 & e^{2\alpha_2 a} & e^{2\beta_2 a} & 1 & 1 & -1 & -1 \\ 0 & \alpha_2 & \beta_2 & 0 & -\alpha_2 & -\beta_2 & \alpha_2 e^{2\alpha_2 a} & \beta_2 e^{2\beta_2 a} & 0 & 0 \\ 0 & 0 & 0 & 0 & \alpha_2 e^{2\alpha_2 a} & \beta_2 e^{2\beta_2 a} & -\alpha_2 & -\beta_2 & \alpha_2 & \beta_2 \\ 0 & \alpha_2^2 & \beta_2^2 & 0 & -\alpha_2^2 & -\beta_2^2 & -\alpha_2^2 e^{2\alpha_2 a} & -\beta_2^2 e^{2\beta_2 a} & 0 & 0 \\ 0 & 0 & 0 & 0 & \alpha_2^2 e^{2\alpha_2 a} & \beta_2^2 e^{2\beta_2 a} & \alpha_2^2 & \beta_2^2 & -\alpha_2^2 & -\beta_2^2 \\ 0 & \alpha_2^3 & \beta_2^3 & 0 & -\alpha_2^3 & -\beta_2^3 & \alpha_2^3 e^{2\alpha_2 a} & \beta_2^3 e^{2\beta_2 a} & 0 & 0 \\ 0 & 0 & 0 & 0 & \alpha_2^3 e^{2\alpha_2 a} & \beta_2^3 e^{2\beta_2 a} & -\alpha_2^3 & -\beta_2^3 & \alpha_2^3 & \beta_2^3 \\ 0 & \alpha_2^4 & \beta_2^4 & 0 & -\alpha_2^4 & -\beta_2^4 & -\alpha_2^4 e^{2\alpha_2 a} & -\beta_2^4 e^{2\beta_2 a} & 0 & 0 \\ 0 & 0 & 0 & 0 & \alpha_2^4 e^{2\alpha_2 a} & \beta_2^4 e^{2\beta_2 a} & \alpha_2^4 & \beta_2^4 & -\alpha_2^4 & -\beta_2^4 \end{bmatrix} \begin{bmatrix} A \\ B \\ C \\ D \\ E \\ F \\ G \\ H \\ I \\ J \end{bmatrix} = \begin{bmatrix} -a \\ -a \\ 1 \\ -1 \\ 0 \\ 0 \\ 0 \\ 0 \\ 0 \\ 0 \end{bmatrix} \bar{p} \tag{5.123}$$

6 Validation Simulations

This section presents numerical simulations that are used to validate tBeam, demonstrate its performance, and explore a beam-to-plate correction factor. tBeam validation is achieved by comparing simulation results with analytical solutions, which are detailed in Section 5. The validation commences with the exploration of an elastic shear beam-foundation system subjected to a uniform load (see Section 6.1). Second, the same beam is subjected to a rolling rigid wheel (in Section 6.2). All examples studied in this report consider loads moving at constant velocities. The velocity is not reported for the elastic cases, Sections 6.1 and 6.2, because the results are independent of the velocity (inertia is ignored in Sections 6.1 through 6.5).

The validation proceeds with the evaluation of viscoelastic (shear) beam-foundation combinations. First, an elastic beam resting on a Kelvin-Voigt foundation is studied in Section 6.3. Next, the Kelvin-Voigt foundation is replaced with a Maxwell foundation in Section 6.4. The validation is concluded, in Section 6.5, with the examination of a Maxwell shear beam resting on a Maxwell Winkler foundation, sharing the same characteristic period. Examples 6.3 through 6.5 consider a rigid wheel loading.

Section 6.6 is used to demonstrate the application of tBeam to study energy dissipation and deflection bowls in realistic pavements. A pavement section designated by the UC Davis Pavement Research Center as PH07 is used for this purpose. A limitation of tBeam is that it employs a one-dimensional beam model to represent a three-dimensional state. This approximation is mandated by the need for highly efficient computations. To compensate for its limitation, the model can be calibrated with a correction factor that can be obtained by comparing the results with more realistic simulations of the three-dimensional pavement structures. As a first step to achieve this goal, Section 6.7 compares tBeam simulations results with those obtained for a two-dimensional plate resting on a Winkler foundation representation.

6.1 Uniform Load on an Elastic Shear Beam-Foundation System

A uniform pressure per unit length is applied to an elastic beam weak in shear resting on an elastic Winkler foundation. The beam's height is 0.2m, and its width is 1m. The beam's material properties are $EI \to \infty$, and $GA_s = 166.66667$N; the stiffness of the Winkler foundation is 166.66667 N/m; and the load $p = -10\ N/m$ is applied to the center 1m portion of the beam.

The tBeam solution is compared with an analytical solution obtained in Section 5. There are two important distinctions between the two solutions. The analytical solution is based on a beam that extends to infinity in either direction, whereas tBeam employs a finite length beam, which in this example extends 20m from the center in each direction. (The load is centered on the beam.) The second difference between the two solutions is that the value $EI = 6.66667E + 5Nm^2$ is used for the tBeam analysis.

tBeam is finite element-based, employing three-node Timoshenko beam elements. The mesh is generated by tBeam as based on the following user input. The beam is to extend 20m in each direction. The center portion of the beam, extending 1m in each direction, from the beam's center, is meshed by 200 elements, with the nodes equally spaced. The exterior segments extending 19m in each direction are mesh by 100 elements with a non-uniform node distribution

done so that intervals between nodes increases as they are further from the center. (Node placement is automatically controlled by tBeam.)

Figure 6.1 shows the distribution of the transverse displacement for the analytical and tBeam solutions. As is evident, a perfect match is obtained. Due to the symmetry of the solution no energy is dissipated in this example.

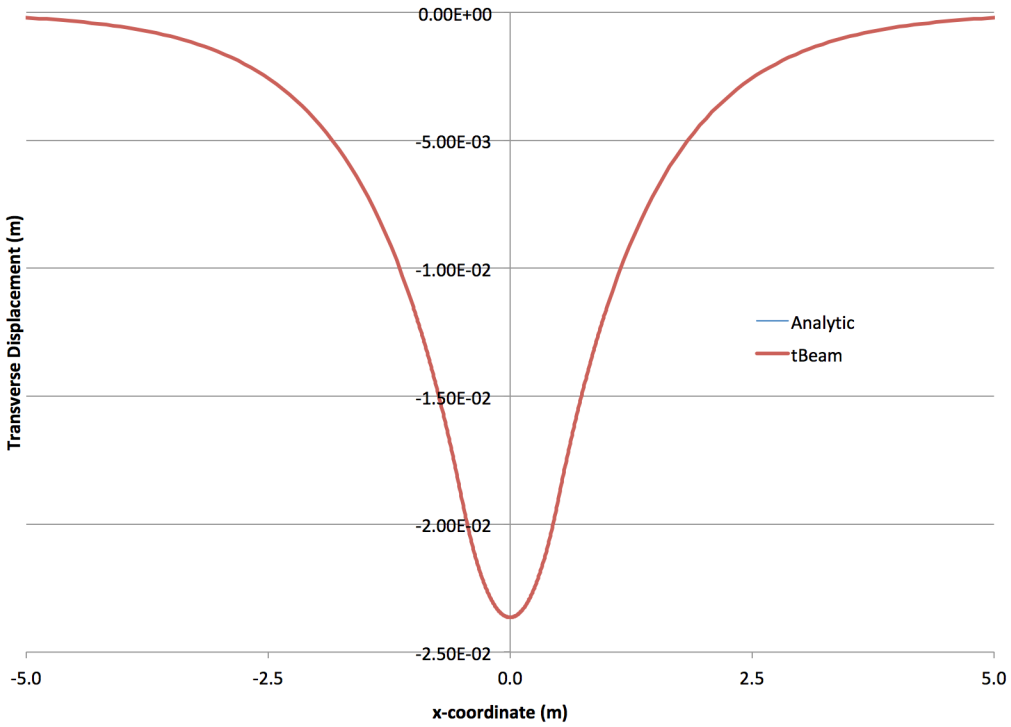

Figure 6.1: Transverse displacement elastic shear beam-foundation system. Uniform load.

6.2 Rigid Wheel on an Elastic Shear Beam-Foundation System

The elastic beam-foundation system considered in the previous example is now subjected to a rolling rigid wheel supporting a vertical force of 10N pointing downwards. The transverse displacement obtained for the analytical solution and tBeam analysis is shown in Figure 6.2. As in the previous example, Section 6.1, the two solutions are practically indistinguishable. No energy is dissipated in this example.

It is also of interest to examine the performance of the contact algorithm. To this end, a close-up view of the wheel-beam system is shown in Figure 6.3. As can be seen, no noticeable penetration is visible. The contact properties used in this example are: $K = 1.0\text{MN/m}$, $p = 2$, and $L_{ref} = 0.002\text{m}$ (see Equation 4.1).

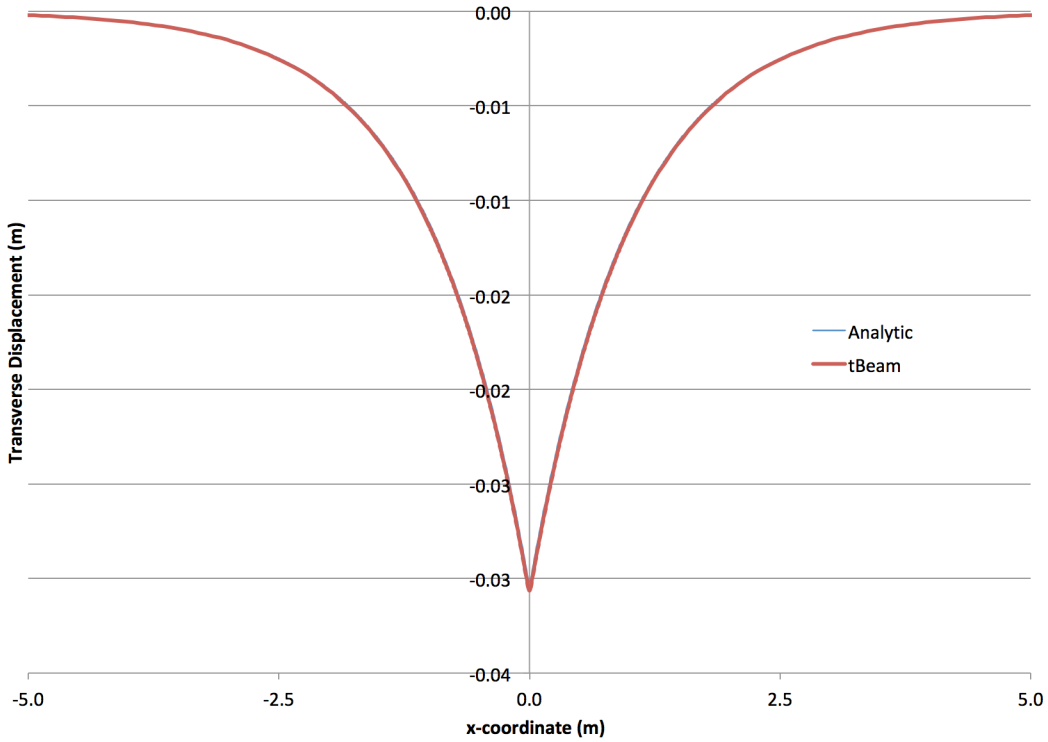

Figure 6.2: Transverse displacement elastic shear beam-foundation system. Rigid wheel.

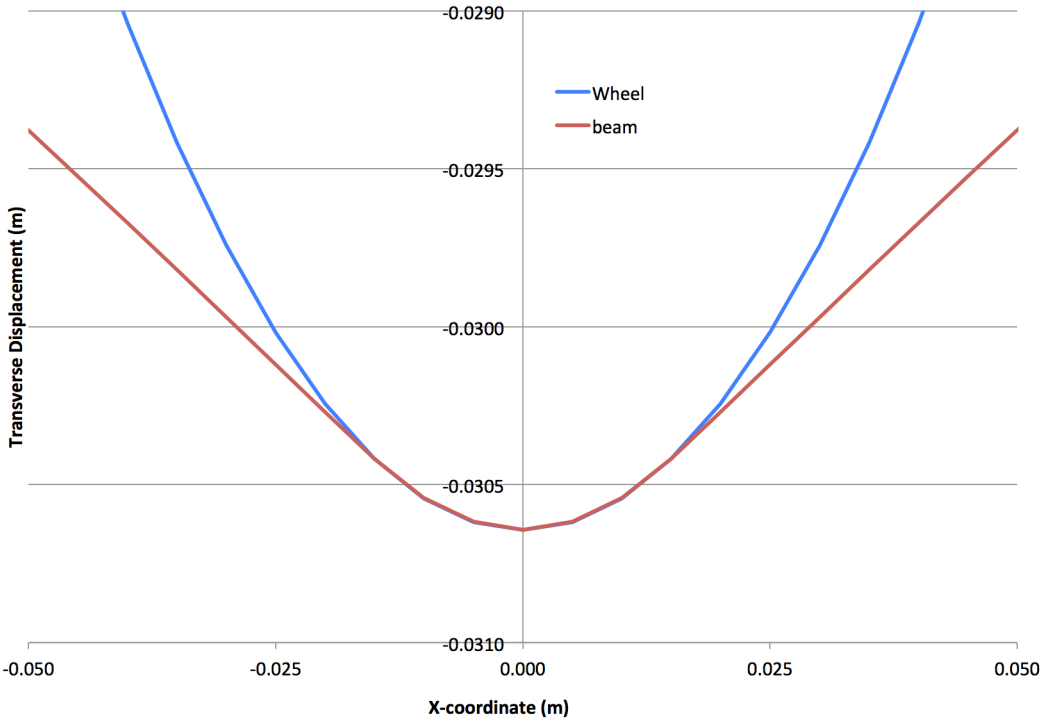

Figure 6.3: Close-up view of the contact zone. Elastic system.

6.3 Rolling Rigid Wheel on an Elastic Shear Beam Resting on a Viscoelastic, Kelvin-Voigt, Foundation

The wheel-beam-foundation system examined in Section 6.2 is reexamined, with the foundation replaced by a Kelvin-Voigt material (see Section 5.3). The spring associated with the foundation is retained, and a dashpot is added in parallel with it to form the Kelvin-Voigt material. The characteristic period for the foundation material is chosen to be 0.1 seconds. The transverse displacement obtained for both analytic and tBeam solutions are shown in Figure 6.3. As in previous sections, the two solutions are indistinguishable.

Figure 6.3 clearly shows that the solution is not symmetric about the center of the beam. This asymmetry results in energy dissipation, which in this case is computed to be 0.142J/m.[5] Figure 6.4 shows a close view of the wheel-pavement contact zone, where no visible penetration is observed. (Contact properties are the same as those used in Section 6.2.)

Section 5.3 introduced the rolling friction resistance, μ. The applied vertical force in this case is 10N. It follows from the definition of the horizontal force, Equation (5.66), that it is equal to the dissipated energy per unit length. Thus, in this example, $\mu = 0.0142$.

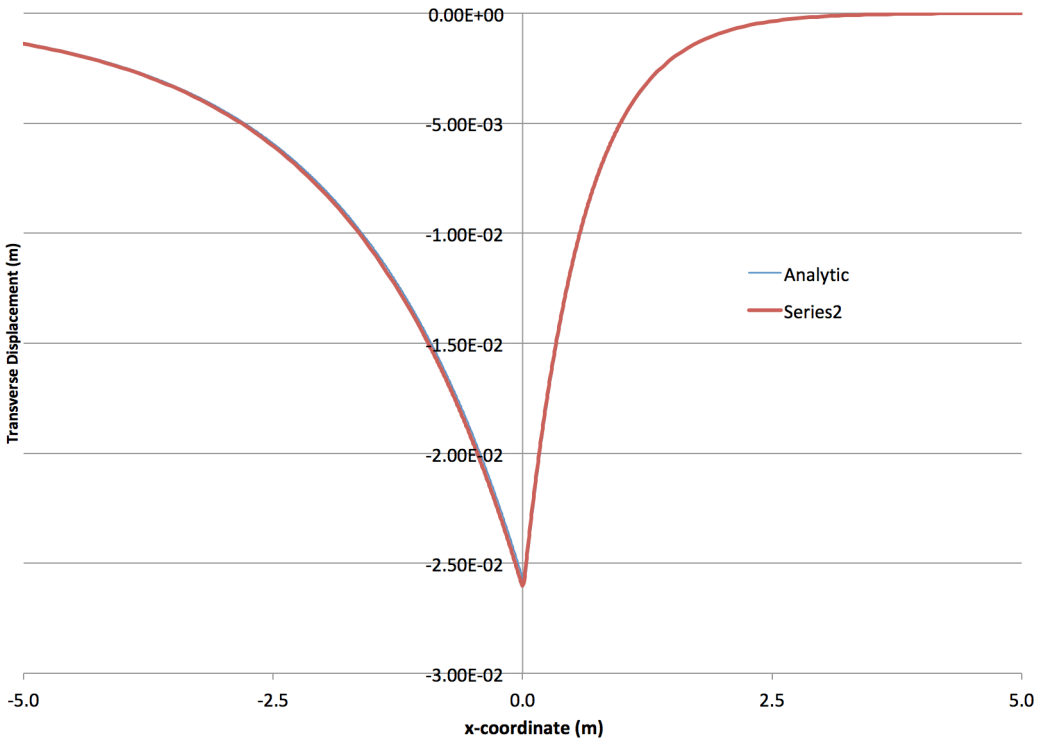

Figure 6.4: Transverse displacement for an elastic shear beam resting on Kelvin-Voigt foundation. Rigid wheel.

[5] The energy dissipated is computed by multiplying the applied (nodal) contact forces by the slope at that node and summing over all the nodes in contact.

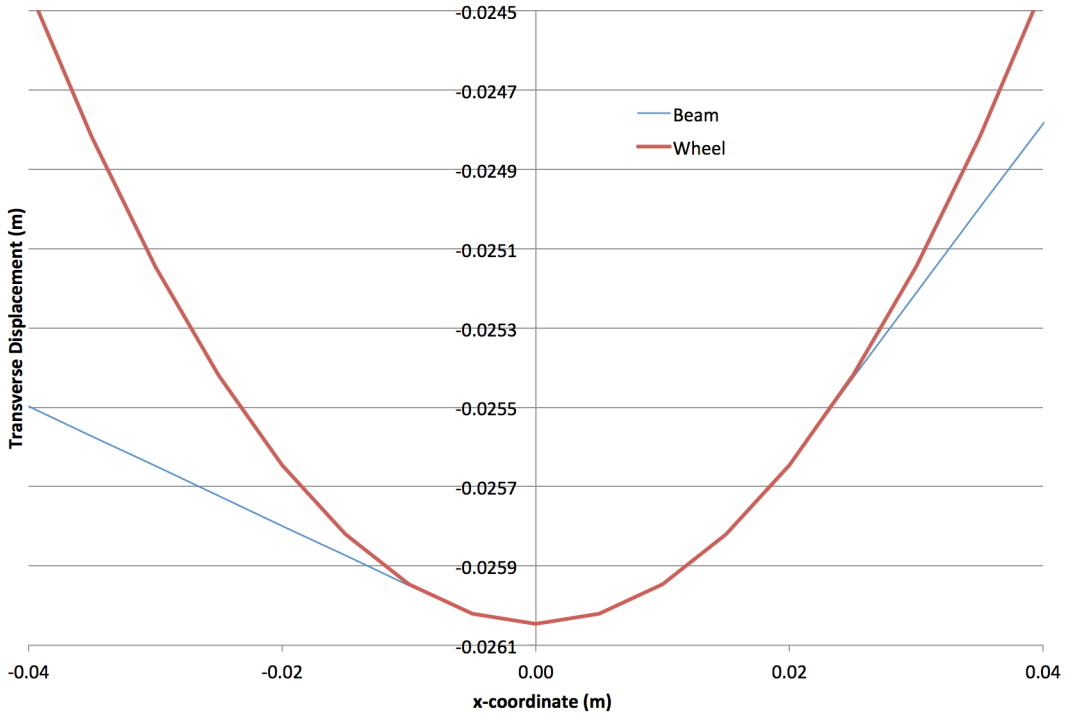

Figure 6.5: Close-up view of the contact zone. Kelvin-Voigt Foundation.

6.4 Rolling Rigid Wheel on an Elastic Shear Beam Resting on a Viscoelastic, Maxwell, Foundation

The wheel-pavement system considered in Section 6.3 is reexamined; this time with the foundation represented as a single Maxwell element. The spring and characteristic period for the Maxwell element have the same properties as those used for the Kelvin-Voigt model in Section 6.3 (*i.e.*, $K = 166.66667 N/m^2$, and $\tau = 0.1$ seconds).

The transverse displacement distributions obtained for the analytic (see Section 5.4) and tBeam solutions are shown in Figure 6.6. This time the tBeam solution does not coincide with the analytical solution. It is, in fact, showing the influence of the finite length of the modeled beam, evident by the curving of the transverse displacement line at both ends of the tBeam solution (L = 20m), an effect that diminishes as the length of the beam is extended. (Recall that the analytical solution assumes a beam that extends to infinity in both directions.)

The elastic bending stiffness of the tBeam model is another factor influencing the closeness of the solution to the analytical solution. Specifically, whereas the analytical solution assumes that $EI \to \infty$, tBeam employs a finite value. As is shown in Figure 6.7, employing a value that resulted in near perfect match, $E = 10^8 N/m^2$, in previous examples did not results in the solutions coinciding in the contact zone in the current example.

As Figure 6.7 shows, even extending the length of the modeled beam to 100m in each direction, marked as L = 100, does not result in the tBeam and analytical solutions coinciding. However, if the bending stiffness is increased, the tBeam solution gets closer to the analytic solution. This is

demonstrated in Figures 6.6 and 6.7 by the curves for a stiffer in bending beam ($E = 10^{12} N/m^2$, L = 100m).

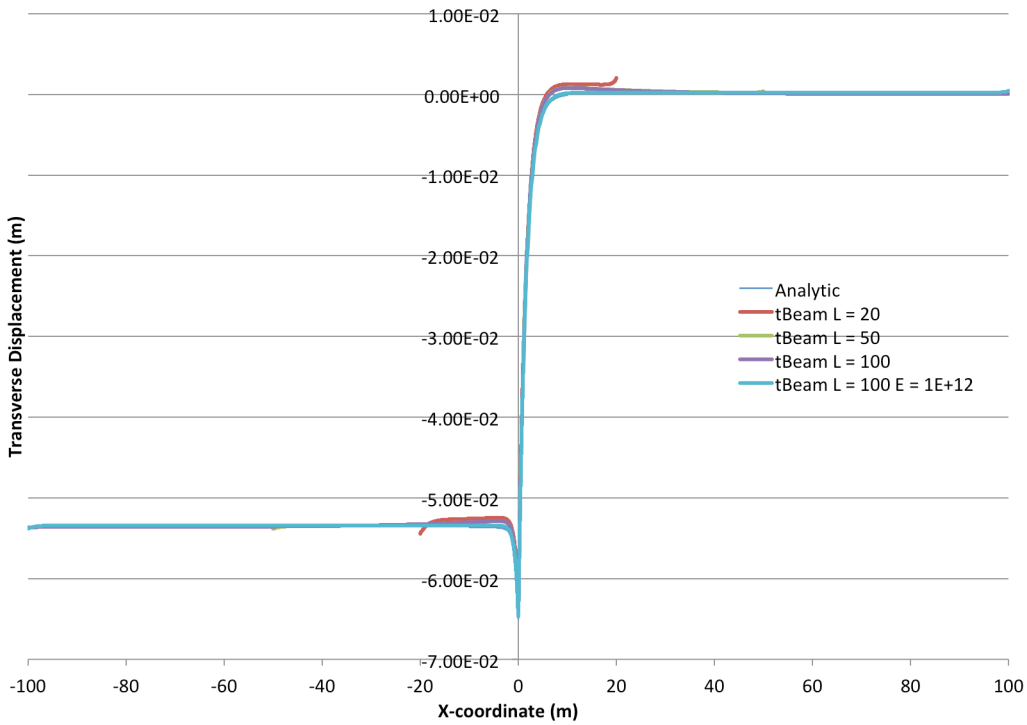

Figure 6.6: Transverse displacement for an elastic shear beam resting on Maxwell foundation. Rigid wheel.

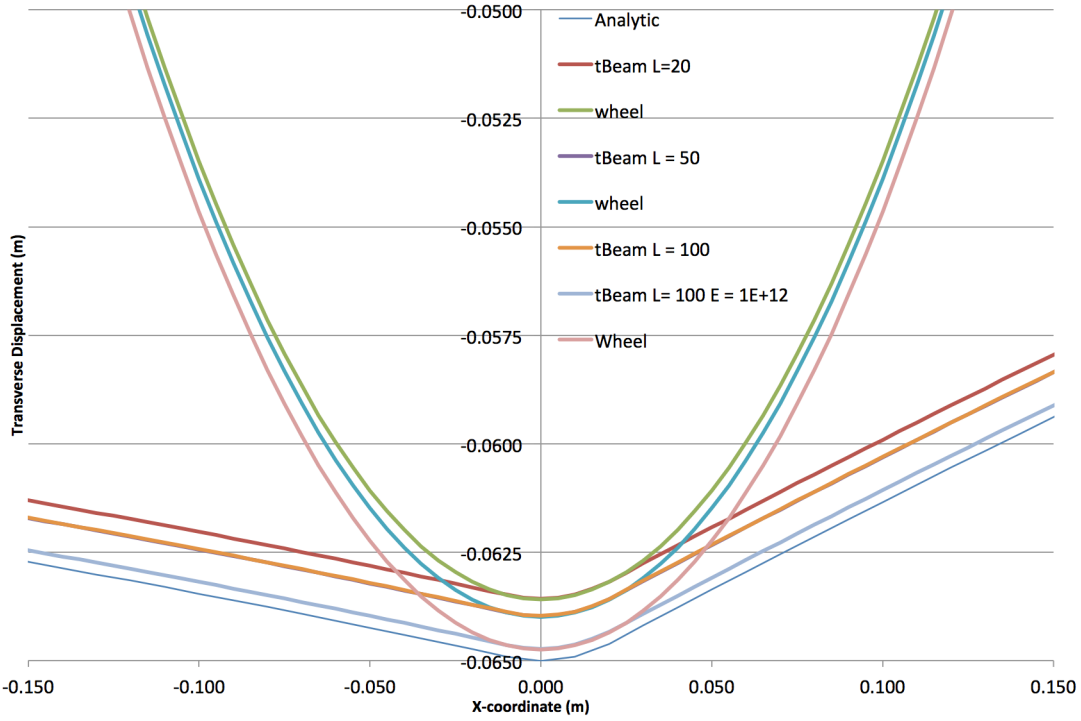

Figure 6.7: Close-up view of the contact zone. Maxwell Foundation.

It is interesting to consider the effect of extending the length of the beam, and increasing the bending stiffness on the dissipated energy. Table 6.1 summarizes the dissipated energy for the cases examined. Fortunately, the dissipated energy is practically unaffected by the end effects, or the bending stiffness.

Table 6.1: Dissipated Energy per unit length. Elastic shear beam, Maxwell foundation.

L (m)	$E(N/m^2)$	Dissipated Energy (J/m)
20	1.0E+8	0.122746
50	1.0E+8	0.122744
100	1.0E+8	0.122703
100	1.0E+12	0.122098

Finally, the horizontal force required to sustain the forward motion is obtained by energy balance (see Section 5). It follows from Equation (5.66) that the magnitude of the horizontal force is the same as that of the dissipated energy per unit length. Thus, in view of the magnitude of the applied vertical force, 10N, the value of the rolling friction resistance is $\mu \approx 0.0122$.

6.5 Rolling Rigid Wheel on a Viscoelastic, Maxwell, Shear Beam-Foundation System

The wheel-pavement system studied in Section 6.4 is enhanced to incorporate viscoelastic response of the shear beam. The model considered contains a single Maxwell element for the shear response of the beam that is chosen to have the same characteristic period as that of the Maxwell element modeling the foundation. The analytic solution for this case is provided in Section 5.5. The properties used for the shear Maxwell element are: $E = 166.66667 N/m^2$ and $\tau = 0.1$ seconds.

Figure 6.8 shows the transverse displacement along the beam. As can be seen, the tBeam and analytic solutions coincide. A close-up view of the contact area is shown in Figure 6.9. The two solutions are indistinguishable also at this scale, and no penetration (wheel-pavement) is visible.

The dissipation computed by tBeam for the applied load of 10N is 0.265767 J/m. Thus, the horizontal force required to maintain the forward motion at 25MPH is 0.265767N, and the rolling friction resistance is $\mu \approx 0.0266$.

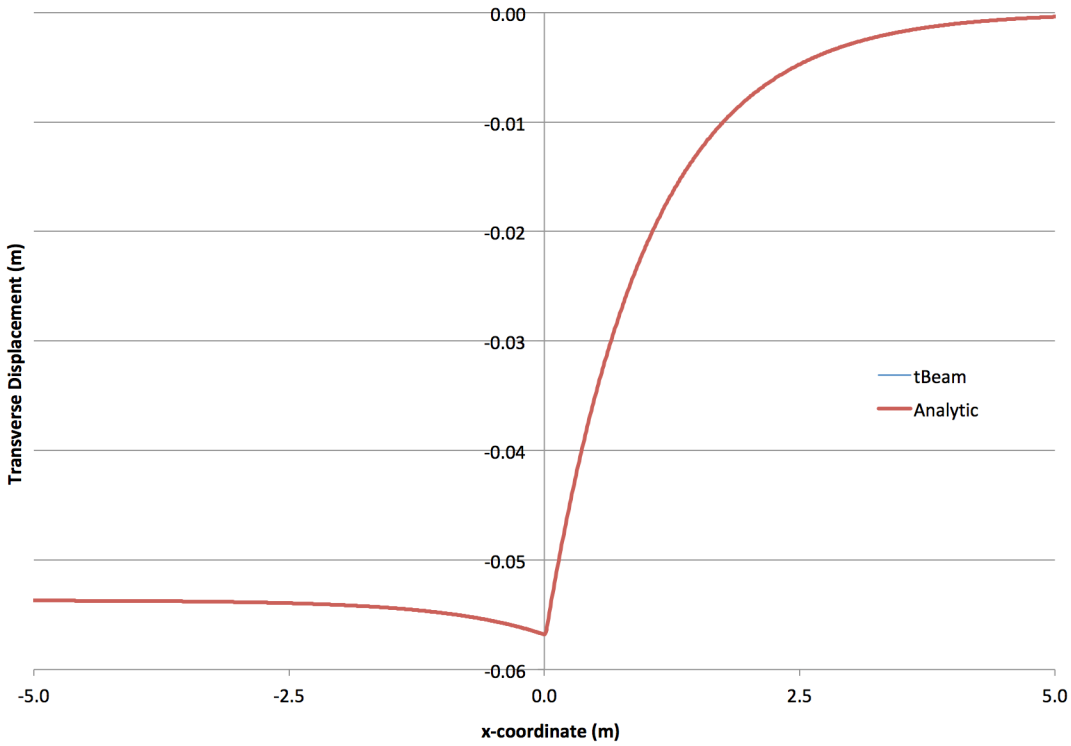

Figure 6.8: Distribution of the transverse displacement along the beam. Maxwell shear beam resting on a Maxwell foundation. Rigid wheel.

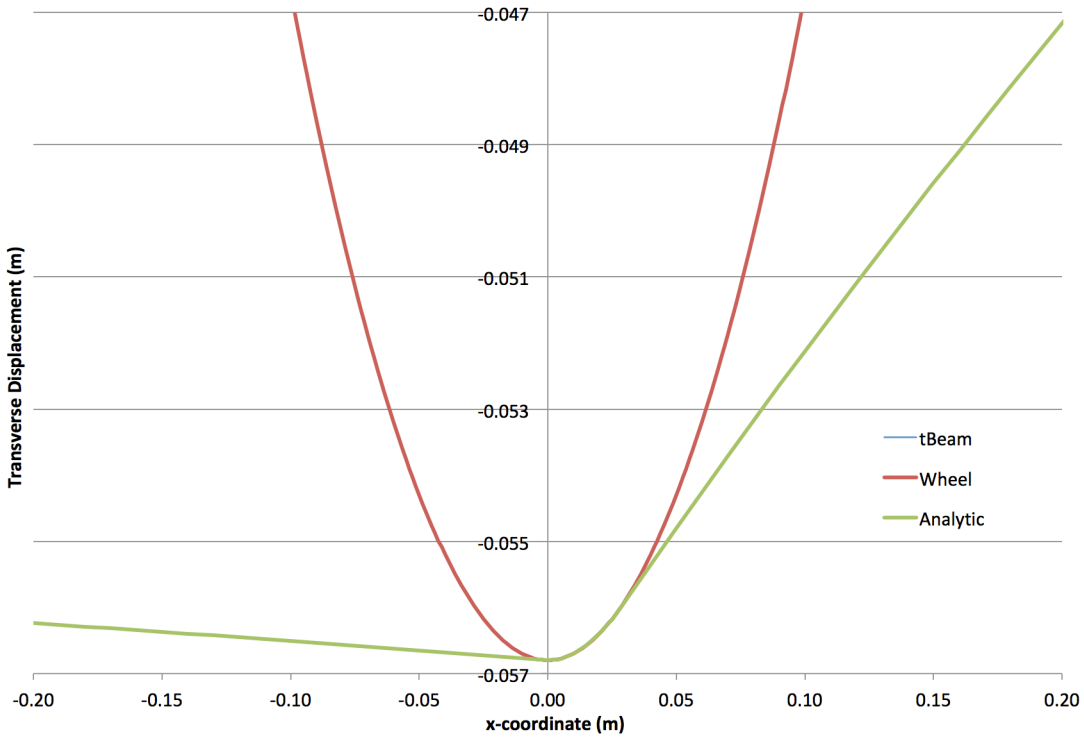

Figure 6.9: Close-up view of the contact area. Maxwell shear beam resting on a Maxwell Foundation. Rigid wheel.

6.6 PH07 Pavement Simulations

The previous simulations, Sections 6.1 through 6.6, were used to validate tBeam. In this section, tBeam is applied to predict the deflection bowl and dissipated energy for a pavement that is designated by the UC Davis Pavement Research center as PH07. The layering for this pavement is provided in Table 6.2. Elastic properties and mass density for the upper three layers are given in Table 6.3. The width of the tBeam model is taken as 1m. This arbitrary beam width is chosen because it is convenient. This issue is further addressed in Section 6.7. Also, note that for uniformly applied pressure, the loading considered here, the transverse displacement and dissipated energy scale linearly with the width.

Maxwell elements (bending and shear) for the top (AC) layer, at the reference temperature of 20°C, are listed in Table 6.4. Scaling factors, used to obtain characteristic periods at different temperatures, are contained in Table 6.5. These scaling factors are uniform (*i.e.*, applied to all Maxwell element, both bending and shear). Finally, the stiffness of the elastic Winkler foundation is $K = 3.11\ 10^8$N/m.

Table 6.2: Pavement section.

Layer	Thickness (m)
AC	0.152
AB	0.3429
ASB	0.279
Foundation	∞

Table 6.3: Layers' Elastic properties and mass density for the upper three layers.

Layer	E (Kg/m^2)	G (Kg/m^2)	Mass Density (Kg/m^3)
AC	2.40E+7	9.00E+6	2304
AB	5.53E+8	1.98E+8	1986
ASB	5.55E+8	1.98E+8	1986

Table 6.4: AC layer's Maxwell elements properties at the reference temperature (20°C).

#	E (N/m^2)	τ (seconds)	G (N/m^2)	τ (seconds)
1	4.7700E+08	5.0E+1	1.7700E+8	5.0E+1
2	9.5800E+09	5.0E+0	3.5500E+8	5.0E+0
3	5.6379E+10	5.0E-1	2.0880E+9	5.0E-1
4	1.2538E+11	5.0E-2	4.6440E+9	5.0E-2
5	1.3877E+11	5.0E-3	5.1390E+9	5.0E-3
6	6.9950E+10	5.0E-4	2.5910E+9	5.0E-4
7	8.6600E+10	5.0E-5	3.2080E+9	5.0E-5

Table 6.5: Scaling (for temperature) factors applied to the characteristic periods.

Temperature (°C)	Scaling Factor
17.1	1.461537636
20.0	1.000000000
27.1	0.224249733
37.1	0.047461069

The load consists of a single wheel, and it is applied as a uniform pressure per unit length, $p = 1.54\ 10^5$N/m, to the center 0.13m of the beam (*i.e.*, $-0.065 \leq x \leq 0.065$). The wheel is moving at either $v = 11.176$m/second (25MPH), or $v = 25.5872$m/second (55MPH). Figures 6.10 and 6.11 show the transverse displacement for the center 20m of the beam for $v = 11.176$m/second and $v = 25.5872$m/second, respectively. (The tBeam model extends in each direction 20m from the center.) As expected, the transverse displacement increases with temperature, and decreases with increased velocity. Figure 6.12 shows the dissipated energy per unit length for the eight cases evaluated.

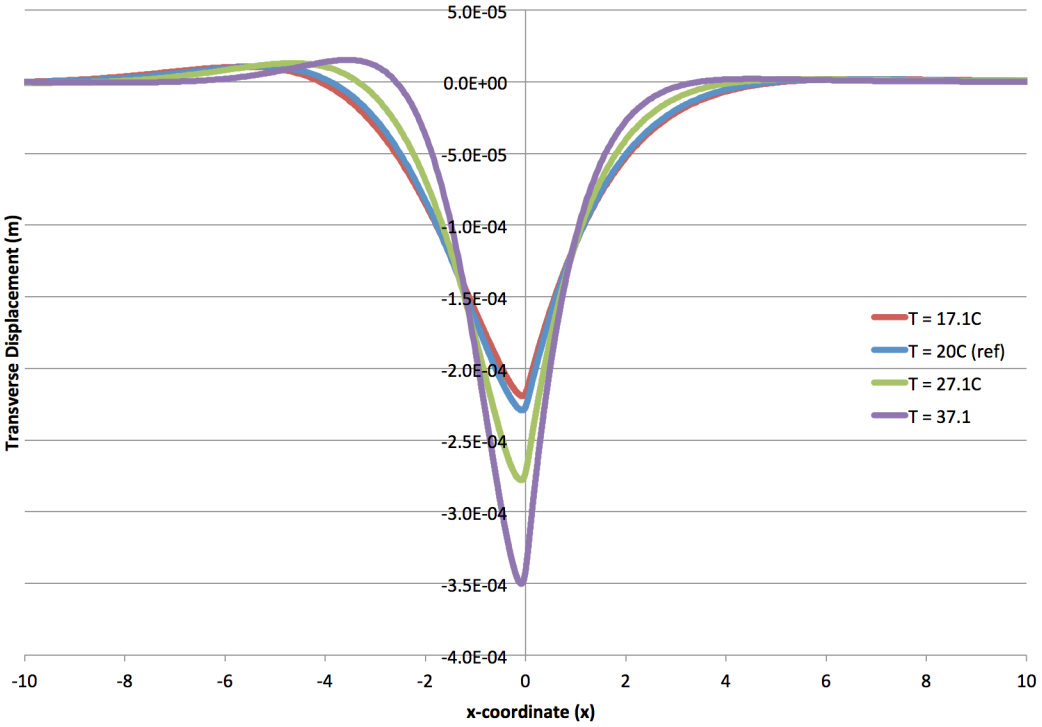

Figure 6.10: Transverse Displacement at $v = 11.176$m/second.

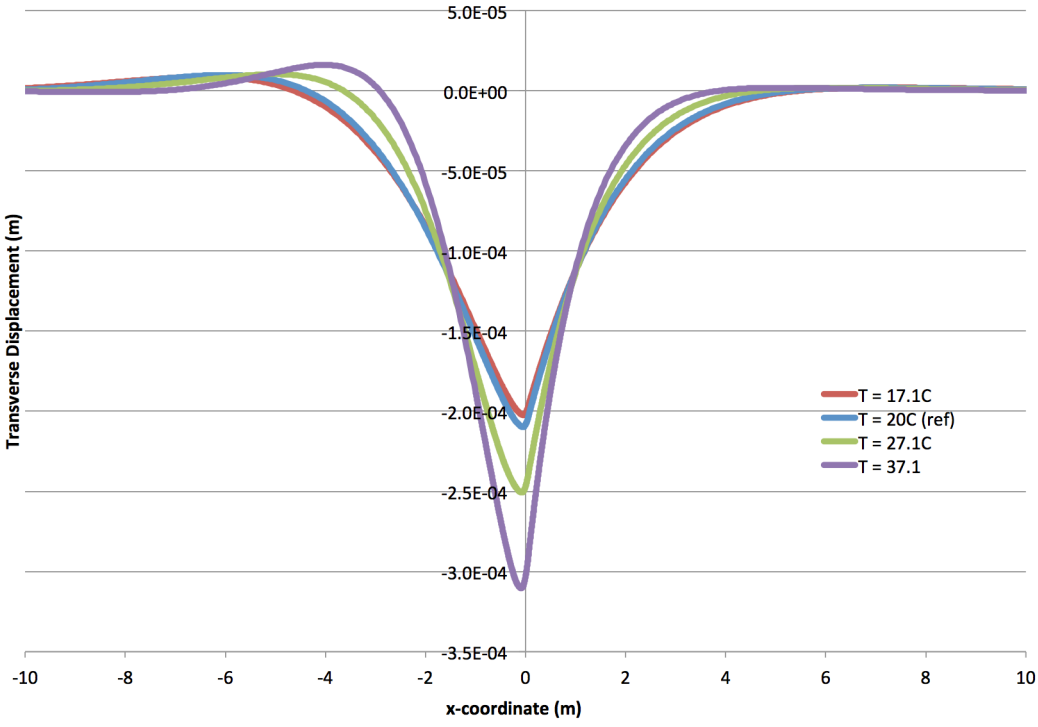

Figure 6.11: Transverse Displacement at $v = 25.5872$m/second.

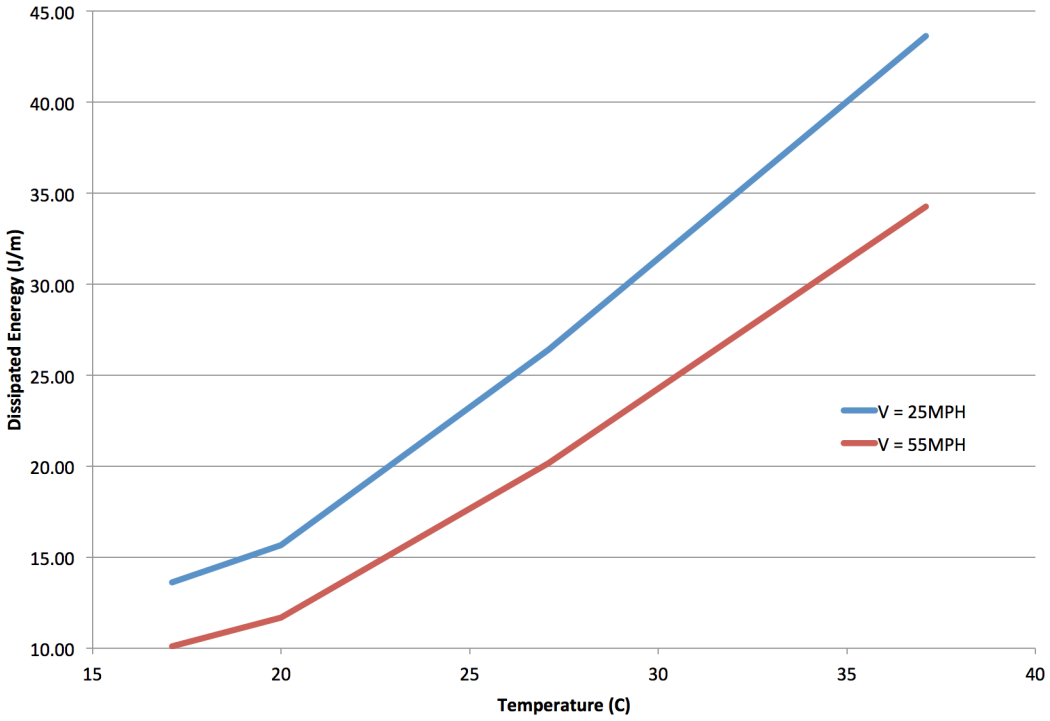

Figure 6.12: Dissipated energy per unit length as a function of temperature.

6.7 Comparison With Plate Analysis

It was noted in the previous example that there is no basis for the choice of the width of the beam. Moreover, the beam model does not account for the double-curvature response of pavements. The objective of this example is to provide a comparison of the beam solution with that of the three-dimensional structure. To this end, a plate model is employed. The plate model is based on the Reissner-Mindlin plate theory and employs the S1 four-node quadrilateral plate formulation (see, *e.g.*, Hughes [1987]). The plate model implementation is designed to represent a single viscoelastic layer resting on a viscoelastic (generalized Maxwell) Winkler foundation. The plate implementation is formulated relative to the inertial coordinate system, and so the load is dragged along the pavement, requiring time integration. Additionally, as the load is coming on the pavement, it causes oscillations of pavement that influence the predicted response. To mitigate these oscillations, light viscosity is added to the foundation.

The properties of the surface layer are the same as those employed for AC layer in Section 6.6. The elastic property of the Winker foundation is the same as that used in Section 6.6. Three Maxwell elements are added to the foundation. Their properties are listed in Table 6.6, and the scaling factors given in Table 6.5 to correct for temperature are applied to the foundation Maxwell elements as well. This scaling is used in order to maintain the light damping for simulations at all temperatures.

Table 6.6: Foundation Maxwell elements properties at the reference temperature (20°C).

#	K (N/m)	τ (seconds)
1	9.0E+6	1.0E+0
2	9.0E+9	1.0E-1
3	9.0E+6	1.0E-2

This example proceeds in two steps. First, tBeam solutions are compared with the plate solution, where the plate is used to model a 1m wide beam and the rotations about the x-axis are fixed in order to closely represent the beam theory. Second, the plate model is used to represent a pavement structure that is 7m wide. (Using symmetry about the x-axis, only the part of the pavement corresponding to the positive y-axis is modeled.) In the axial direction (*i.e.*, direction of motion), the pavement model extends 5m in each direction from the center. The load is moved from $x = -5.065$m to $x = 0$m in five thousand time steps, whose size depends on the velocity of the wheel. Two velocities are considered: $v = 11.176$m/second (25MPH) and $v\,25.5872$m/second (55MPH). Additionally, the analyses are repeated at three temperatures: 17.1°C, 27.1°C, and 37.1°C.

The deflection bowls at the three temperatures considered are shown in Figures (6.13-6.15) (25MPH) and (6.16-6.18)(55MPH). They follow the expected trend of increasing transverse deflection with rising temperature, and lower velocity. It is evident, however, that the plate model representing the bar and tBeam do not coincide, with the difference being considerably smaller for the higher velocity. This difference is likely due to two sources. First, the constitutive model for the plate is not identical to that for the bar. Specifically, the plate model introduces certain couplings that are not present in the beam model. Even in the restricted case of linear elastic response, the difference vanishes only for zero Poisson's ratio. Second, tBeam employs quadratic elements, whereas the plate model employs bi-linear elements. This approximation difference results in more elements required for the plate model to achieve the same accuracy. However, the two-dimensional memory requirement (the model used about half a million degrees of freedom) restricted the mesh size employed.

The purpose of the one-dimensional (bar) analysis with plate elements was to enable comparison with the two-dimensional (plate) analysis when using identical formulations. Examining the results shows that the two-dimensional results in significantly lower transverse displacement, especially at lower temperatures and higher velocities. This result is attributed to two reasons: the arbitrary unit width of the one-dimensional model and the double-curvature effect present in the two-dimensional analysis.

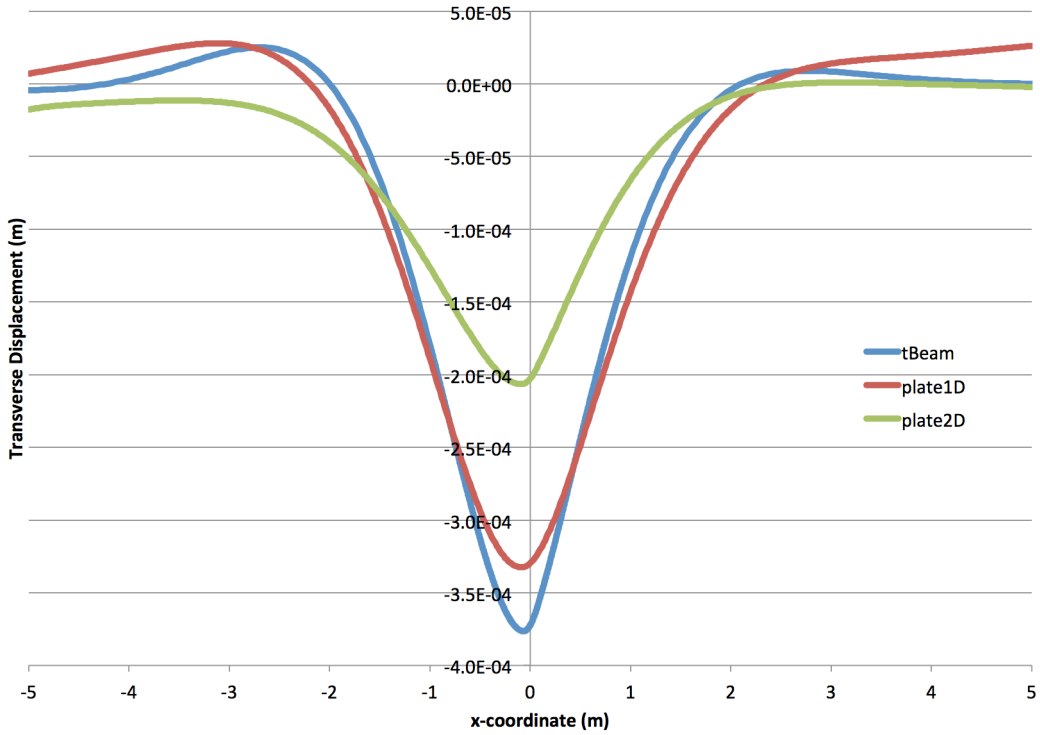

Figure 6.13: Transverse Displacement at $v = 11.176$m/second, T=17.1°C.

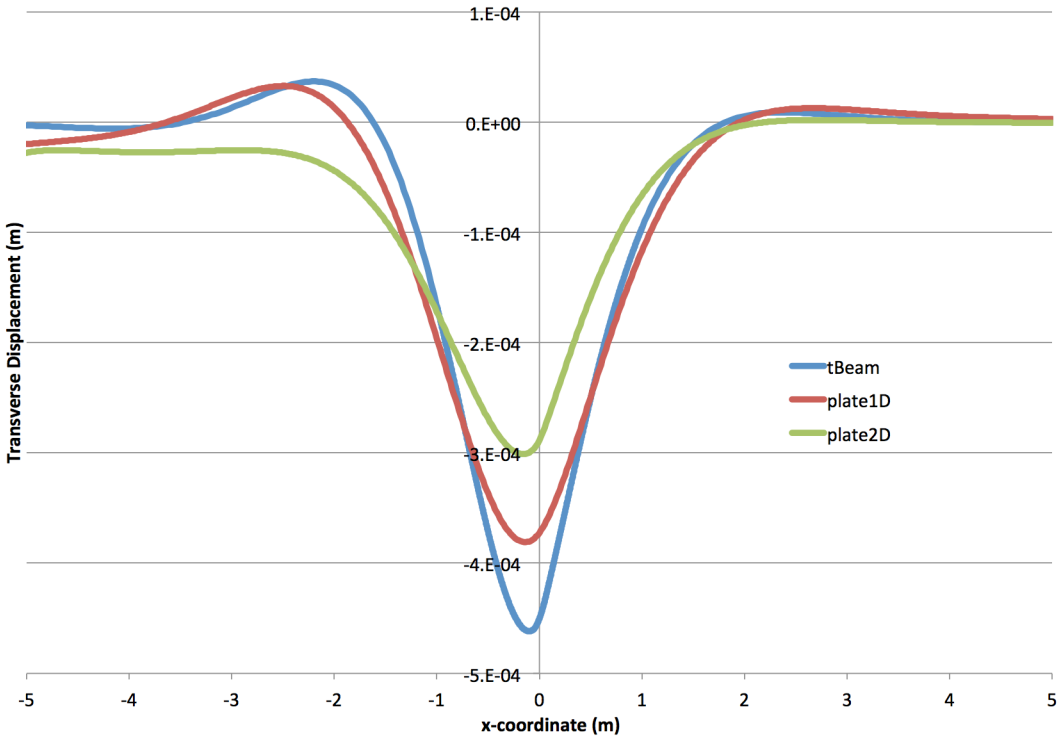

Figure 6.14: Transverse Displacement at $v = 11.176$m/second, T=27.1°C.

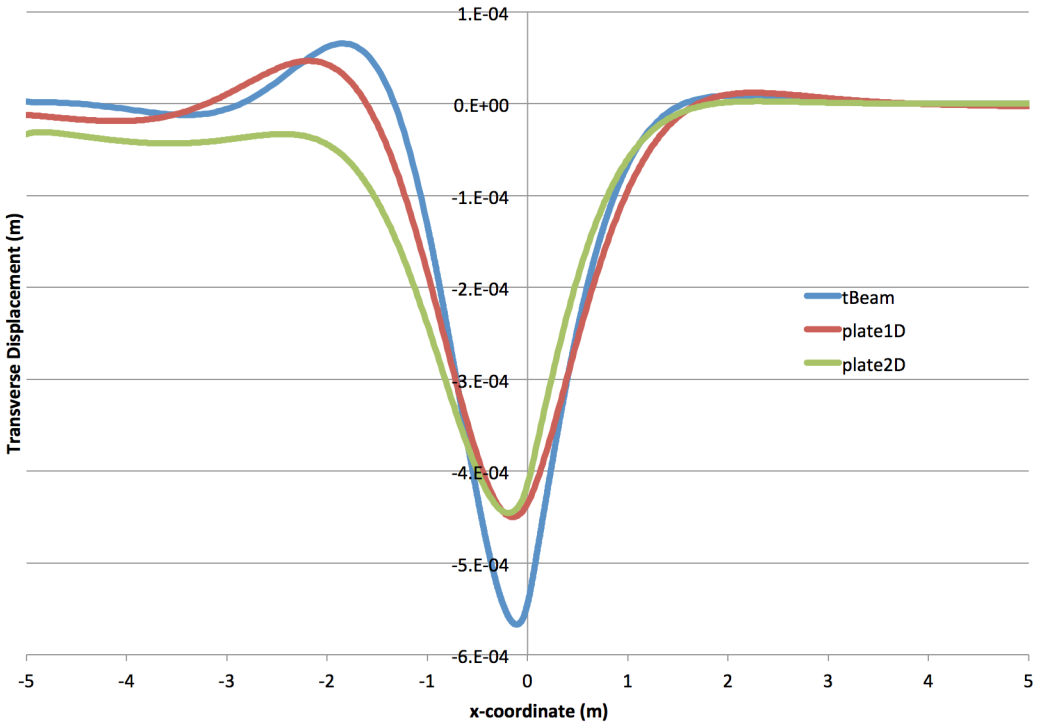

Figure 6.15: Transverse Displacement at $v = 11.176$m/second, T=37.1°C.

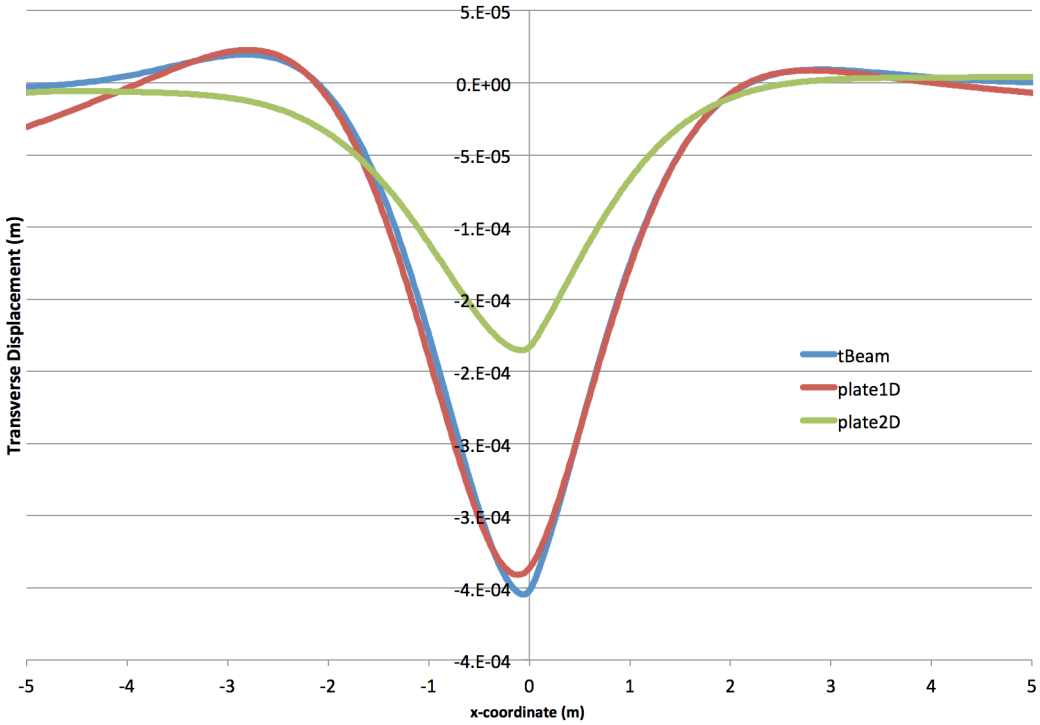

Figure 6.16: Transverse Displacement at $v = 25.5872$m/second, T=17.1°C.

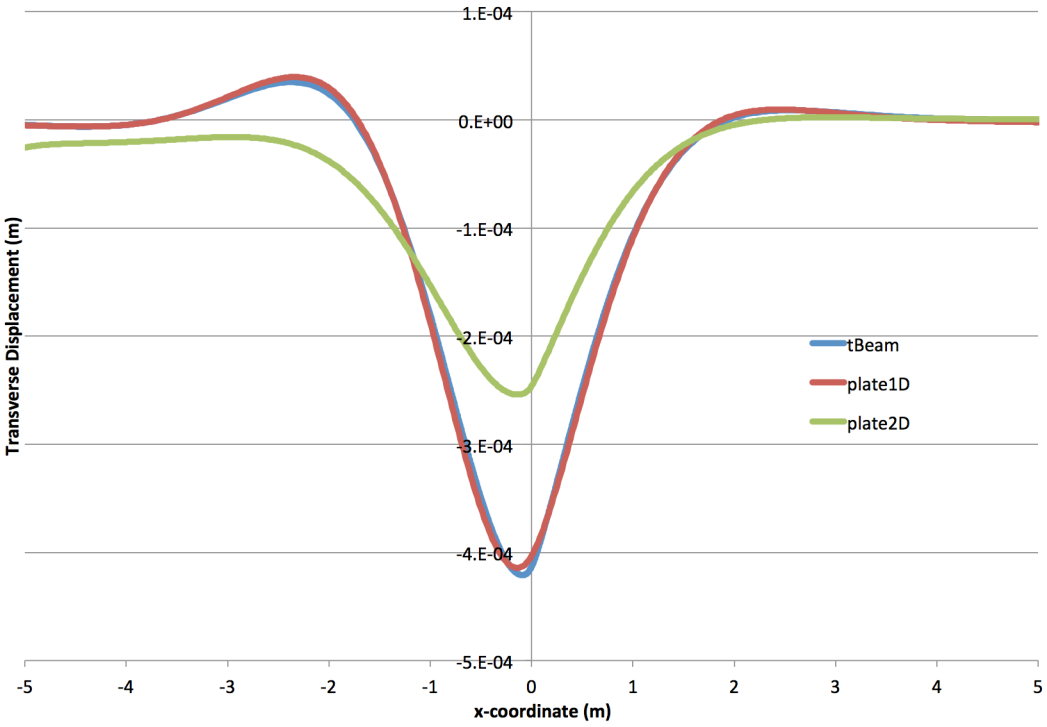

Figure 6.17: Transverse Displacement at $v = 25.5872$m/second, T=27.1°C.

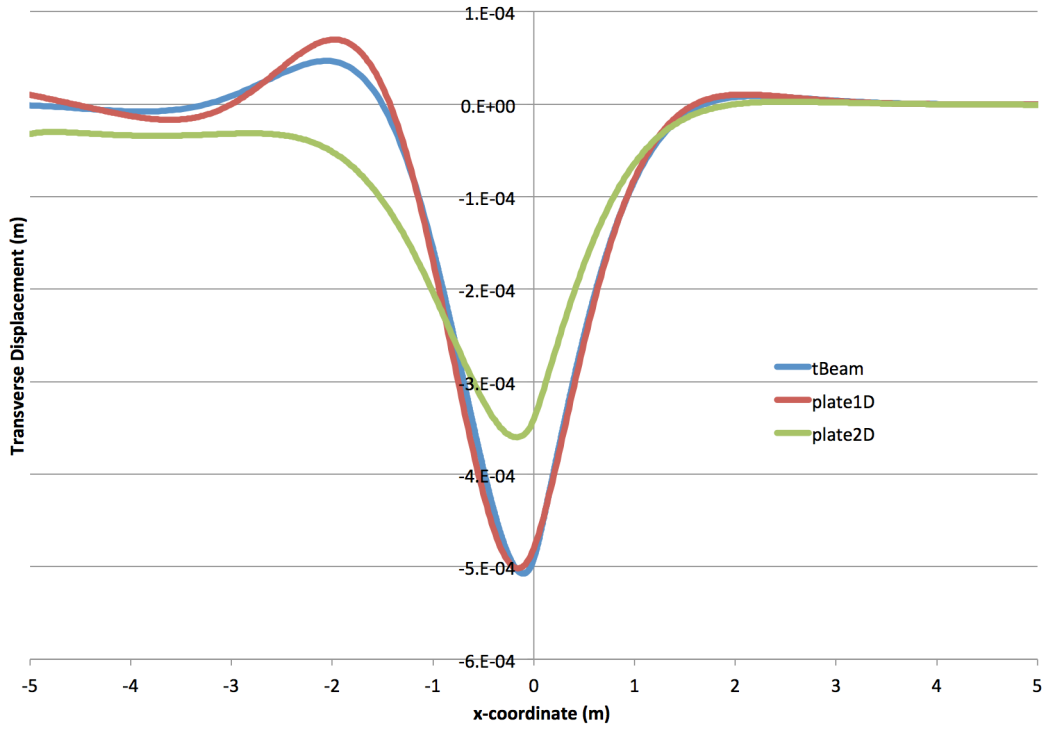

Figure 6.18: Transverse Displacement at $v = 25.5872$m/second, T=37.1°C.

The dissipated energy *vs*. temperature for the two velocities studied is shown in Figures (6.19) ($v = 11.176$m/second) and (6.20) ($v = 25.5872$m/second). The results show that the dissipated energy increases with rising temperature and decreases with increased velocity. This outcome is consistent with physical observations. The results also show that tBeam dissipated more energy than either of the plate analyses. The relationship between the one- and two-dimensional analyses is not consistent. At the lower velocity, the two-dimensional analysis dissipated more energy, whereas at the higher velocity the one-dimensional analysis dissipated more energy. This result is best viewed by examining the ratio of dissipated energy for one- to two-dimensional analyses, shown in Figure 6.21. The results show a clear trend of increased ratio with reduced velocity and increased temperature. However, more analysis is needed in order to arrive at a correction factor, even restricted to this case.

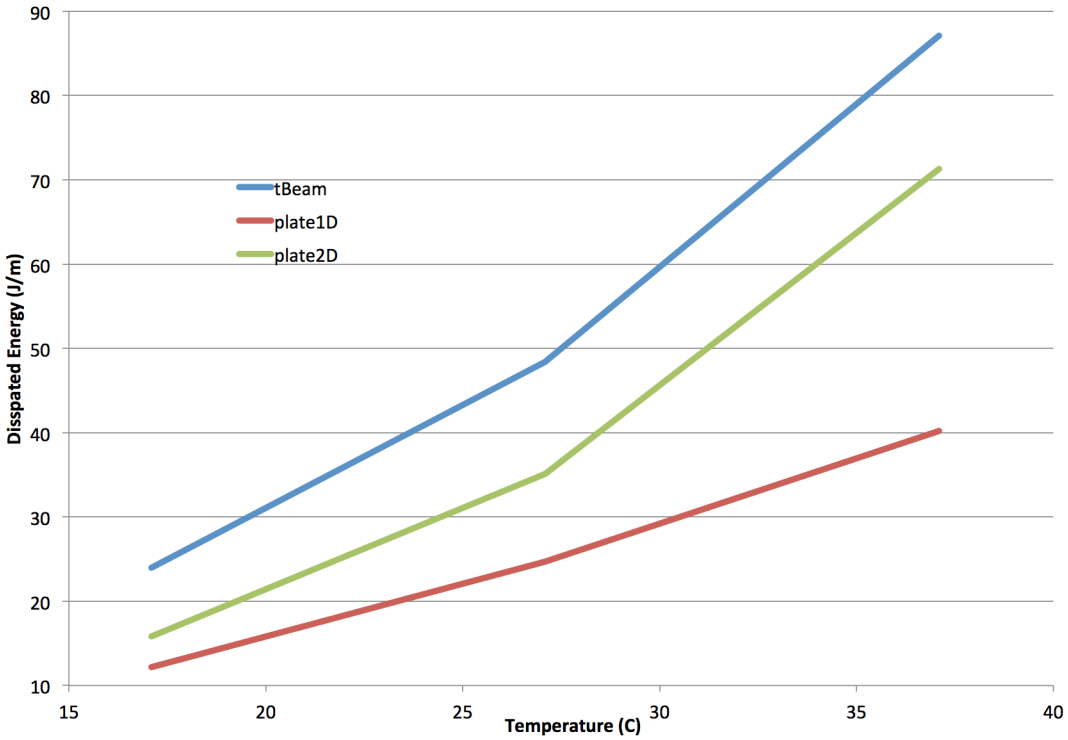

Figure 6.19: Dissipated energy *vs*. temperature ($v = 11.176$m/second).

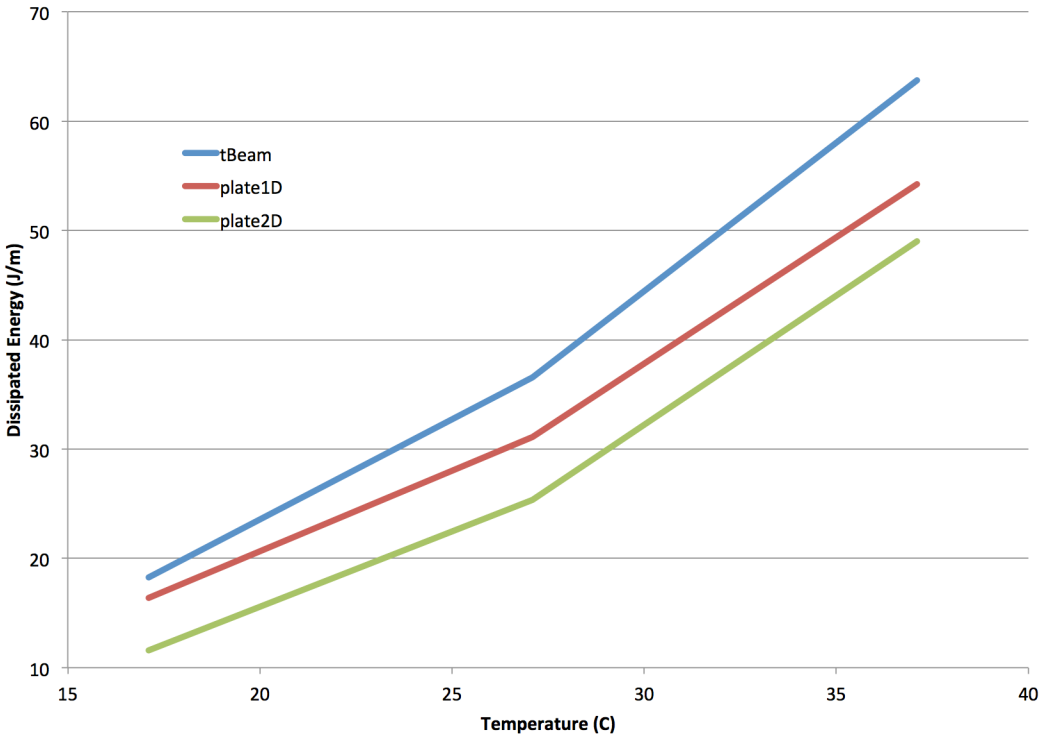
70
60
50
40
30
20
10
15
20
25
30
35
40
Dissipated Energy (J/m)
Temperature (C)
tBeam
plate1D
plate2D

Figure 6.20: Dissipated energy *vs*. temperature ($v = 25.587$m/second).

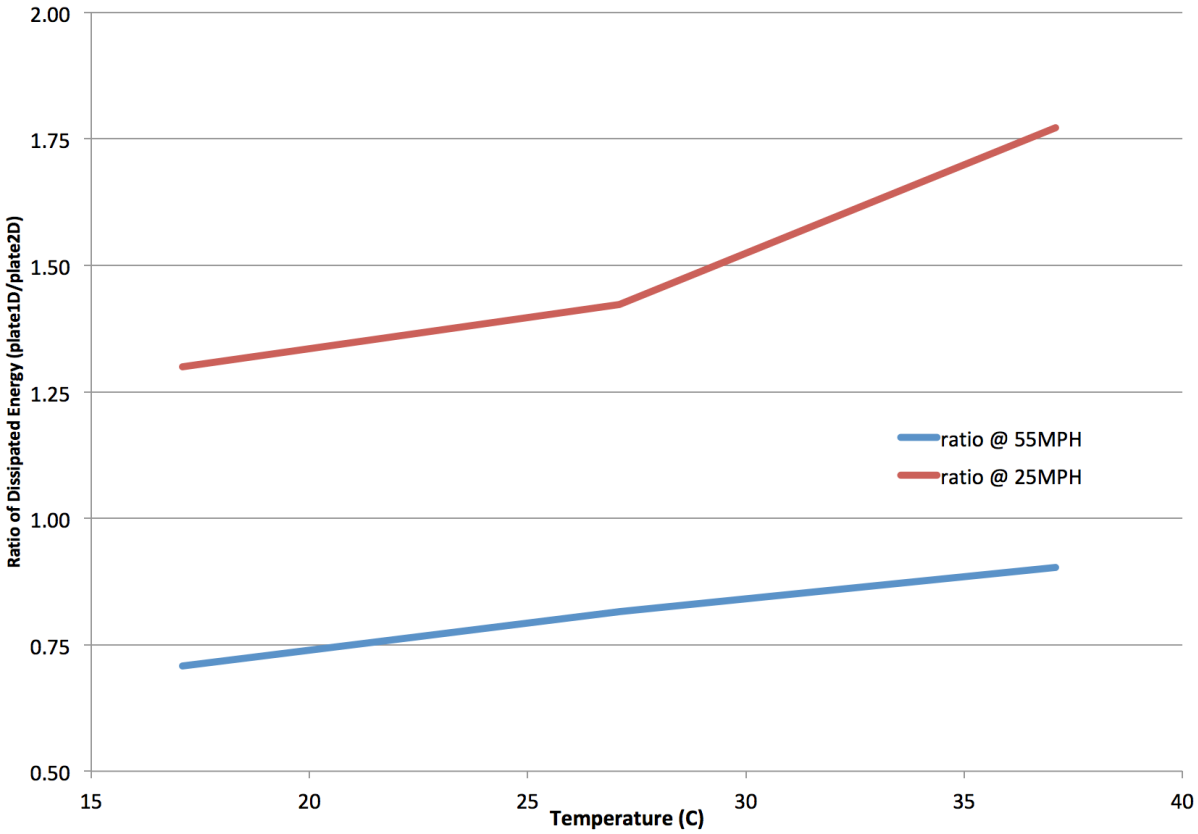

Figure 6.21: Ratio of dissipated energy for plate models (1D/2D).

7 Conclusions and Future Work

This report presents the theoretical background for tBeam, a program for the analysis of deflection bowls and energy dissipated in viscoelastic pavement structures. tBeam is finite-element-based and employs a one-dimensional multilayered linear viscoelastic Timoshenko beam model resting on a linear viscoelastic Winkler foundation. Both the beam (shear and bending components) and foundation are modeled by generalized Maxwell element representations.

This report also presents a number of closed-form analytical solutions for a number of combinations of material models of a beam weak in shear resting on Winkler foundation. These analytical solutions are then used for the tBeam validation effort, which is also contained in this report. Additionally, an example of the application of tBeam to a realistic pavement section is provided.

A shortcoming of the use of a one-dimensional model is that it cannot capture the double-curvature effect present in real pavements. Applying a correction factor to the tBeam results can mitigate this shortcoming. To this end, tBeam results are compared with those obtained for a plate model of a simple pavement structure. The results establish a clear trend where the correction factor decreases with temperature and increases with wheel velocity. Unfortunately, the current study is insufficient to establish a clear law to determine the correction factor, even when limited to the case studied, and further analysis is need.

In running validation examples, a problem was encountered with the representation of the "stand-alone" dashpot in the beam (shear and bending components). This problem is related to the appearance of a higher order derivative coupled with multiplication by the negative of the velocity (see the transformation from Equation (2.10) to Equation (2.14)). Fortunately, a simple workaround is readily available in the form of adding a Maxwell element with a stiff spring, and characteristic period such that the desired dashpot viscosity is obtained.

As pointed out in the introduction, numerical efficiency is critical for the integration of tBeam with pavement sustainability analysis software. This need mandates that, within the confines of this application, applying the load as a uniformly distributed pressure is preferable to the simulation of the rigid wheel-pavement contact. Moreover, because the indentation is very small relative to the radius of the wheel, the resulting contact area is only a fraction of the real contact area, which also favors applying the load as a uniformly distributed pressure.

Finally, the following future undertakings are suggested:

- A relation between the tBeam predicted energy dissipation and the predicted energy dissipation when accounting for the three-dimensional nature of the pavement system could be determined. In essence, this study would be an expanded version of the example provided in Section 6.6. The outcome of this study will be a function to correlate tBeam predictions with three-dimensional response for a range of pavement structures, loading, temperatures, and vehicle velocities.
- Applying the load as a uniformly distributed pressure over a specified contact area can be easily changed to account for non-uniform distribution. This change would require the user to

input the details of the distribution, but otherwise it will have no impact on the numerical effort.

- A deformable wheel can replace the rigid wheel model employed by tBeam. In this case, a beam model will be used to represent the steel-reinforced rubber tire and the internal pressure will be applied as a "follower pressure" (*i.e.*, the pressure would remain normal to the beam). This enhancement will result in a more realistic prediction of the contact area. Unfortunately, it will add to the numerical cost of the analysis. Therefore, such an enhancement would primarily benefit pavement research.
- tBeam can be enhanced to better account for the three-dimensional response of pavements. This enhancement would employ a formulation based on the shear deformable Reissner-Mindlin plate theory. To maintain efficiency, it too will be formulated relative to a moving coordinate system. Additionally, it would employ a regular finite element representation in the direction of motion (same as tBeam), and a prescribed shape function in the (in-plane) normal direction. Such an approach would be almost as efficient as tBeam, yet account for the double curvature nature of the response. This tool would benefit both pavement research and sustainability analysis.

References

Hughes, T.J.R., [1987], *The Finite Element Method, Linear Static and Dynamic Finite Element Analysis*, Prentice-Hall, Inc. Englewood Cliffs, New Jersey.

Hughes, T.J.R., R.L. Taylor, J.L. Sackman, A. Curier, and W. Kanoknukulchai, [1976], "A Finite Element Method for a Class of Contact-Impact Problems," *Computer Methods in Applied Mechanics and Engineering*, 8: 249-276.

Kelly, J.M., [1962], "Moving Load Problems In the Theory of Viscoelasticity, Ph.D. Dissertation, Stanford University, April.

Taylor, R.L., [1985], "Solution of Linear Equations by a Profile Solver," *Engineering Computations*, 2: 344-350.

Timoshenko, S.P., [1921], "On the correction factor for shear of the differential equation for transverse vibrations of bars of uniform cross-section," *Philosophical Magazine*, 41: 744-746.

Timoshenko, S.P., [1922], "On the transverse vibrations of bars of uniform cross-section," *Philosophical Magazine*, 43: 125-131.